University of Windsor

Scholarship at UWindsor

8-15-2019

Spray Characteristics of Dimethyl Ether in a Direct Injection Application

Simon LeBlanc
University of Windsor

Follow this and additional works at: https://scholar.uwindsor.ca/etd

Spray Characteristics of Dimethyl Ether in a Direct Injection Application

By

Simon LeBlanc

A Thesis
Submitted to the Faculty of Graduate Studies
through the Department of Mechanical, Automotive and Materials Engineering
in Partial Fulfillment of the Requirements for
the Degree of Master of Applied Science
at the University of Windsor

Windsor, Ontario, Canada

2019

Spray Characteristics of Dimethyl Ether in a Direct Injection
Application

By

Simon LeBlanc

APPROVED BY:

_____
Dr. Xueyuan Nie
Department of Mechanical, Automotive & Materials Engineering

_____
Dr. Nick Eaves
Department of Mechanical, Automotive & Materials Engineering

_____
Dr. Jimi Tjong, Co-Advisor
Department of Mechanical, Automotive & Materials Engineering

_____
Dr. Ming Zheng, Co-Advisor
Department of Mechanical, Automotive & Materials Engineering

August 15, 2019

DECLARATION OF ORIGINALITY

I hereby certify that I am the sole author of this thesis and that no part of this thesis has been published or submitted for publication.

I certify that, to the best of my knowledge, my thesis does not infringe upon anyone's copyright nor violate any proprietary rights and that any ideas, techniques, quotations, or any other material from the work of other people included in my thesis, published or otherwise, are fully acknowledged in accordance with the standard referencing practices. Furthermore, to the extent that I have included copyrighted material that surpasses the bounds of fair dealing within the meaning of the Canada Copyright Act, I certify that I have obtained a written permission from the copyright owner(s) to include such material(s) in my thesis and have included copies of such copyright clearances to my appendix.

I declare that this is a true copy of my thesis, including any final revisions, as approved by my thesis committee and the Graduate Studies office, and that this thesis has not been submitted for a higher degree to any other University or Institution.

ABSTRACT

The primary objective of this thesis is to analyze the spray characteristics and behaviour of dimethyl ether (DME) in a high-pressure direct injection application. To achieve these results, two optically-accessible constant-volume chambers (CVC) will be used to observe the fuel spray development. An injector is instrumented inside the CVC and the injections are recorded with a high-speed camera. Various injection and background parameters are manipulated to study the effect of each parameter on the fuel spray characteristics and spray behaviour. Two types of experiments are used to study fuel spray, a quantitative study and an observational study. The first uses a direct imaging setup to measure the spray characteristics, e.g. spray penetration length and cone angle. The latter adopts a shadowgraph imaging technique to enhance the visual representations of vaporization around the fuel spray.

In the first section of results, only the spray characteristics and vaporization behaviour of DME fuel will be presented and detailed. These will include results from both experiment types, the quantitative study and the observational study.

In the second section of results, the corresponding sprays of diesel and n-butanol fuel are analyzed and compared to that of DME fuel. For a thorough comparison of the tested fuels, these experiments are subjected to the same testing parameters as used for DME fuel.

DEDICATION

This work is dedicated to my sister, my parents,

and my beloved brother-in-law.

Forever in my heart.

ACKNOWLEDGEMENTS

TABLE OF CONTENTS

LIST OF TABLES

LIST OF FIGURES

xi

NOMENCLATURE

CI	Compression Ignition	
CO	Carbon Monoxide	
COV	Coefficient of Variation	[%]
CR	Compression Ratio	[-]
CVC	Constant-Volume Chamber	
DI	Direct Injection	
DME	Dimethyl Ether	
DOC	Diesel Oxidation Catalyst	
EGR	Exhaust Gas Recirculation	
EOI	End of Injection	
FPGA	Field-Programmable Gate Array	
HCCI	Homogeneous Charge Compression Ignition	
HP	High-Pressure	
IC	Internal Combustion	
IPoD	Injector Power Driver	
LHV	Lower Heating Value	[MJ/kg]
LNT	Lean NOx Trap	
LTC	Low-Temperature Combustion	
NOx	Nitrogen Oxides	
PFI	Port Fuel Injector	
PM	Particulate Matter	

ROI   Rate of Injection

RT   Real-time

SCR   Selective Catalytic Reduction

SCRE   Single Cylinder Research Engine

SI   Spark Ignition

SOI   Start of Injection   [°CA]

TDC   Top Dead Centre

THC   Total Hydrocarbons

CHAPTER I

INTRODUCTION

The objective of this work is to analyze the spray characteristics of dimethyl ether (DME) fuel injection at high-pressures. Further, the empirical results are compared with that of n-butanol and diesel fuel. The comparisons are made in regards to spray penetration length, spray cone angle, and vaporization characteristics. The study will be used to form a database for the application of DME fuel in a direct injection (DI) compression ignition (CI) engine.

1.1 Research Background

The goal of an internal combustion (IC) engine is to convert the fuel energy into useful work. Numerous methods of combustion have been investigated and applied since the invention of the IC engine. The two primary combustion methods are CI and spark ignition (SI). Specific amounts of oxygen, fuel, and ignition energy are required to achieve complete combustion. Two popular methods of supplying fuel involve fuel injection into the intake manifold and directly into the cylinder. A port fuel injector (PFI) is used to inject fuel into the intake port to mix with fresh air before entering the cylinder. Auto-ignition of the mixture takes place only after a portion of the vaporized fuel is mixed with the air within the flammability limits and the local temperature is above the auto-ignition temperature [1]. A fully homogeneous yet lean mixture can be achieved using a PFI, typically resulting in low-temperature combustion (LTC) in a compression ignition set-up [2,3]. The main advantage of an LTC mode is the ultra-low in-cylinder NOx and dry soot

emissions in compression ignition engines [4]. LTC can be divided into numerous categories, one being homogeneous charge compression ignition (HCCI) [5,6]. In an HCCI type of combustion, the fuel and air are premixed so that a near homogeneously charged mixture is available for combustion. A major limitation is the lack of direct control on the ignition timing, as the combustion is solely reliant on the fuels' auto-ignition properties and the chemical kinetics of the mixture [5,7–9]. Conversely, a conventional DI-type combustion mode allows for control through means of diesel injection timing.

Fossil fuels have been the main energy sources for combustion in engines since the beginning of the mass-production of on-road vehicles [10]. Conventionally, gasoline and diesel fuels operate under two different combustion methods, i.e. spark ignition and compression ignition. Important in-cylinder combustion characteristics, such as the ignition delay and the combustion duration, are heavily reliant on fuel properties, specifically the Cetane number and Octane number [4]. Typical gasoline fuels, being highly volatile, with high-Octane numbers and low-Cetane numbers, have great mixing characteristics that facilitate the suitable application in SI engines. In SI engines, both the fuel and air are introduced from the intake port to the cylinder and, after compression, electric energy is used to initiate the combustion via a spark plug arc. On the other hand, diesel fuels, with low-Octane numbers and high-Cetane numbers, have low auto-ignition temperatures, making it suitable for CI engines. CI engines draw in solely air during the intake stroke. Since the intake air charge is not combustible, CI engines can use higher compression ratios (CR) than that of SI engines, theoretically increasing the potential thermal efficiency of the combustion cycle [4]. The in-cylinder gas is then compressed as the piston moves towards the top dead centre (TDC) to reach a sufficient temperature,

higher than the auto-ignition point of the mixture. The diesel fuel is subsequently injected into the hot and oxygen abundant environment, which initiates auto-ignition in the locally near-stoichiometric air-fuel mixture. This injection process of diesel fuel leads to the diffusion (or mixing-controlled) combustion because of the limited time for the air-fuel mixing prior to the initiation of the combustion. Typically, the diffusion burning produces more smoke than the premixed combustion [6,11]. The locally fuel-rich conditions are difficult to avoid when the air-fuel mixing process takes place in the course of diffusion burning. Traditional CI engines emit significantly larger amounts of particulate matter (PM) than that of SI engines. At the same time, the locally near stoichiometric burning generates high flame temperatures and produces high NOx emissions [12]. Unfortunately, the technologies adopted for NOx reduction often result in an increase in the PM [13].

The government continuously tighten the regulations on harmful emissions, including PM, NO_x, carbon monoxide (CO), total hydrocarbons (THC), and CO_2. Currently, both aftertreatment and in-cylinder strategies are used to minimize the tail-pipe emissions. Catalytic converters are the common after-treatment tools implemented to reduce exhaust emissions. Catalytic converters commonly used on diesel engines include a selective catalytic reduction (SCR), lean NO_x trap (LNT), and diesel oxidation catalysts (DOC). Unfortunately, these additions increase cost, complexity, and some impose fuel efficiency penalties [13–18]. The technique of exhaust gas recirculation (EGR) is useful to lower the local flame temperature, thus to reduce NOx emissions [3,7,8,19–23]. EGR is applied in modern engines by routing a portion of the exhaust gases into the intake manifold. Though EGR is effective in reducing NOx emissions, it may increase soot emissions. In order to overcome the infamous trade-off between NOx and soot emissions, local flame

temperatures must be kept low and the homogeneity of the air-fuel mixture must be enhanced. One approach to obtain sufficient fuel-air mixing is to replace the diesel fuel with an alternative fuel that has a high oxygen content and volatility, such as n-butanol and DME.

1.2 Alternative fuels

The use of alternative fuels in combustion can be a solution to improving engine-out emissions. Many alternative fuels have been investigated in the past [24]. These studies detail the feasibility, production (source and quantity), combustion abilities, and emission characteristics for uses in on-road vehicles. The key properties of diesel and gasoline fuels, alongside the popular alternative fuels, are tabulated in Table 1.1. Alcohols, alkanes, and ethers are all potential fuels for engine applications, each type with their own respective advantages and disadvantages. Another advantage of using alternative fuels is to have the potential to contribute toward issues such as the reduction of carbon dioxide (CO_2) and the improvement of energy sustainability and security [25]. In this work, DME and n-butanol are selected as the research fuels of interest, both possessing certain properties suitable for clean combustion and fuel-air mixing.

1.2.1 Dimethyl Ether

Dimethyl ether (DME) is an oxygen-borne fuel with promising potential, including the ability to be a bio-renewable source of energy [26–29]. This fuel is used for numerous applications, depicted in Figure 1.1. The molecular structure (CH_3-O-CH_3) of this neat fuel is vastly different from that of diesel fuel ($C_nH_{1.8n}$), wherein it lacks carbon to carbon bonding and has an oxygen atom. The use of DME in a diesel engine can yield comparable

energy efficiency with significantly improved smoke emissions [26,27,30,31]. Even under diffusion burning, due to the extremely high fuel volatility along with the hefty fuel-borne oxygen (34.8% by mass), the DME combustion typically produces near-zero smoke [32–36]. Sato *et al* investigated the performance of DME in a light-duty truck [37]. The authors describe that DME promises smoke-free combustion, with a reduction in NO_x emissions by 40 percent compared to that of diesel combustion under the same conditions. Huang *et al* conducted engine tests using DME with EGR in a modified DI CI engine; they were able to reduce NO_x levels further by applying EGR, without affecting the ultra-low soot emissions [18]. However, a number of limitations arise in the DME fuel substitution.

Applications	Usages
Household	Aerosol and propellant sprays Freeze spray (mixed with LPG) Cooking fuel Cosmetics
Transportation	Diesel engines Passenger vehicles
Industry	Power generation Refrigerant Direct oxidation of fuel cells Solvent for extraction of organic compounds
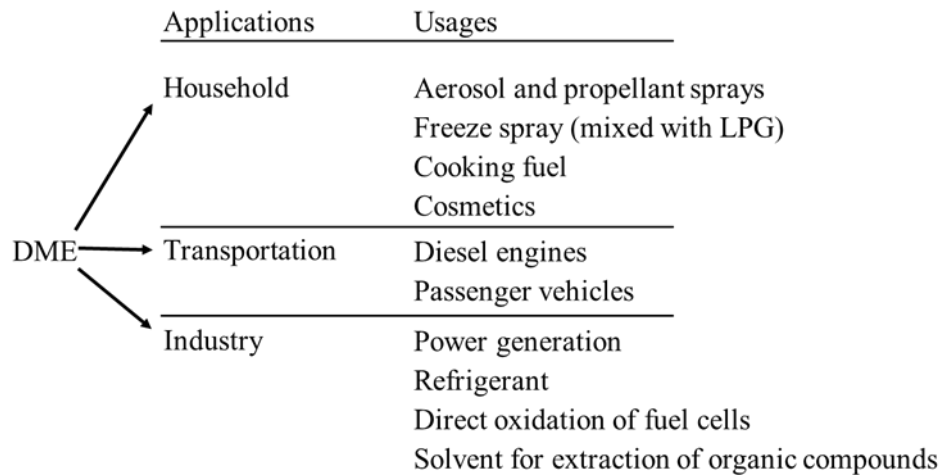
Figure 1.1 Applications of DME [26,38–40]

The implementation of DME as an alternate fuel for DI has limitations that must be taken into account. One of the major differences between DME and other liquid alternative fuels is the boiling point at 1 bar absolute pressure (atmospheric pressure). The phase diagram for DME is shown in Figure 1.2. Under 1 bar absolute, DME is in a gaseous state. This is an issue for pumping since liquid fuel is required for high-pressure DI injection. Therefore,

the devising of a pressurized fuel return line to maintain DME fuel at liquid phase is required. To account for the heating and safety factors of the DME fuel, it is reported that a closed-loop fuel system under 31 bar absolute is appropriate [41]. Other limitations include the need to add a lubricant enhancer to DME fuel for the application in currently-used high-pressure injectors.
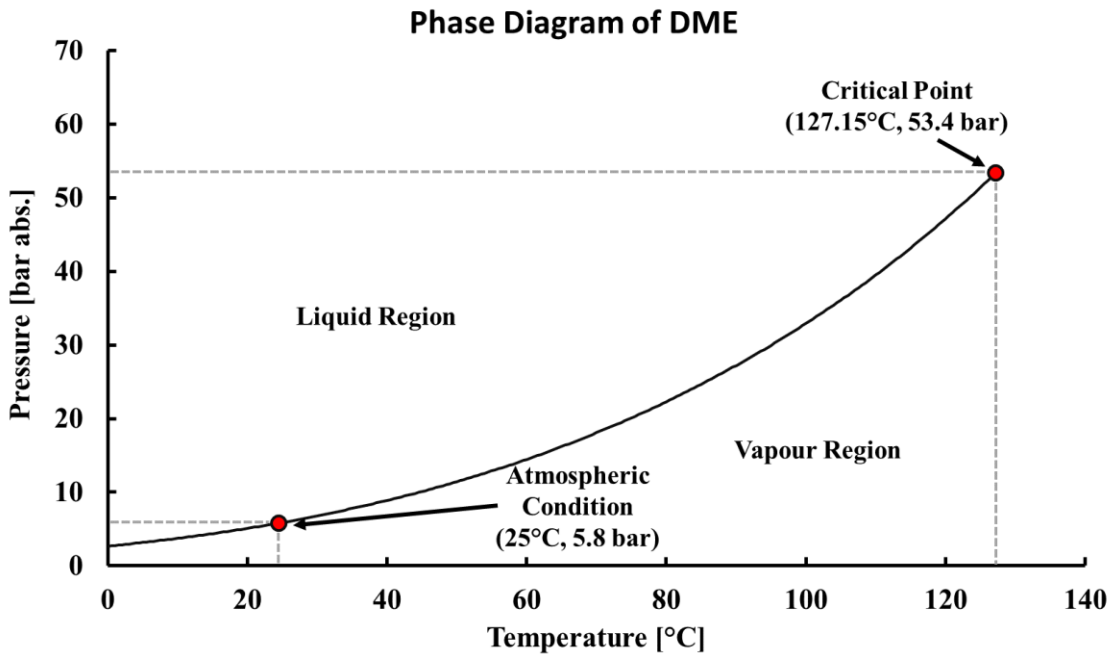
Figure 1.2 Phase diagram of dimethyl ether [28]

1.2.2 n-Butanol

n-Butanol fuel, a single component liquid which can be made from bio-stock, possesses attractive properties as a substitution to diesel fuel in combustion [25,42,43]. Biofuels such as n-butanol are among the leading contenders to replace petroleum fuels in the transportation sector for their potential to use the existing powertrain designs and refuelling infrastructures. The volatility of n-butanol is greater than diesel and its Cetane number is lower, allowing more time to mix and achieve a more homogeneous mixture of fuel and

6

air. Additionally, n-butanol can be used in blends with diesel at different fuel ratios to study engine performance and exhaust emissions [12,44–47]. Yanai *et al* investigated the performance using neat n-butanol in a DI CI engine at low-loads [48]. The authors detailed that very low NOx and soot emissions were produced. However, hydrocarbon and carbon monoxide emissions were greater than those of diesel because of the longer ignition delay and the lower combustion temperature of n-butanol. It was suggested that these challenges can be addressed using various strategies, including EGR, multiple injections, and a cetane number improver [48].

Table 1.1 Properties of Conventional Alternative Fuels [13,27,38,41,49–55]

Properties	Units	Diesel	Gasoline	DME	n-Butanol
Chemical formula	-	$C_nH_{1.8n}$	$C_nH_{1.87n}$	CH_3OCH_3	$n-C_4H_9OH$
Cetane number	-	43	10-17	55-60	17-25
Octane number	-	25	87	13	87
Molecular weight	g/mol	~170	~110	46	74
Stoichiometric air/fuel mass ratio	kg/kg	14.6	14.8	8.95	11.2
LHV	MJ/kg	43	43	28.4	33.1
Oxygen content	wt %	0	0	34.8	21.6
Liquid kinematic viscosity	cSt	>3	0.4-0.8	0.184	3.6
Liquid density @ 15 °C	kg/m^3	840-880	720-780	667@5 bar abs	810
Auto-ignition T.	°C	180-285	220-260	350	340
Heat of evaporation	kJ/kg	316.6	303	465	595
Surface tension @ 25 °C	mN/m	24	22	11	25
Modulus of elasticity (x10^8)	N/m^2	14.86	*adequate*	6.37	*adequate*
Lubricity, HFRR WSD* [55]	μm	300@60 °C	700-900@25 °C	*poor*	622
Vapor pressure @ 20 °C	kPa	<< 10	70	510	2.07
Boiling T. @ 1 bar abs	°C	180-360	60-200	-25	117.5

* High-Frequency Reciprocating Rig, Wear Scar Diameter

1.3 Spray Characteristics

The spray process is inherently chaotic and random in nature [56]. In order to characterize the fuel spray by high-pressure injection, two parameters are commonly measured, i.e. the spray penetration length and the spray cone angle [56]. In a DI engine, the overpenetration of the spray leads to the impingement of fuel on the cylinder walls, known as wall-wetting. If the walls are not sufficiently hot to trigger autoignition, this phenomena may result in higher THC emissions, poor mixing, and lower fuel economy [4,56,57]. Additionally, a larger spray cone angle leads to improved mixing capability. Due to the wider spray dispersion, the fuel spray has more contact area with the fresh-air. The fuel behaviour at high injection pressures is primarily affected by the fuel properties, especially the kinematic viscosity and the surface tension [56]. Several experimental and simulation studies have been performed with the objectives of understanding DME and its spray characteristics [32,33,58–60].

Yu *et al* conducted spray experiments in an optically-accessible constant-volume chamber (CVC) to observe the spray characteristics of DME under various injecting pressures and background conditions [58]. The authors compared the results to that of the diesel fuel and two popular spray models, Dent's model [61] and Hiroyasu & Arai's model [62]. The research [58] concluded that the appearance of gaseous DME spray was eminent under 1 bar absolute background pressure and the spray cone angle was expanded as a result of flash boiling atomization. However, an increase in background pressure (above 31 bar absolute) caused DME to remain liquid during injection, resulting in a spray cone angle no longer affected by any noticeable flash boiling effects. The increase in the background

pressure led to similar spray developments as diesel fuel. The authors suggested that the DME spray is likely to have greater ignitability due to a vaporizing region around the plumes that tended to increase with the fuel injection pressure.

S. C. Sorenson *et al* tested DME fuel injection in a single-hole nozzle injection system using Schlieren setup, a modified shadowgraph imaging technique [59]. The authors detailed that the compression work required for pumping liquid DME can be 3.2 times that of liquid dodecane, a representative of diesel fuel [63], owing to the lower liquid density and higher compressibility of DME. It was concluded that the observable spray behaviour of DME is similar to that of diesel, based on Schlieren photography. On the other hand, the vaporization of DME spray is more rapid than diesel fuel under background pressure conditions above 15 bar. The spray breakup was observed for all DME cases, in which the spray tip or side of the main plume separated and quickly evaporated. In the same way, lateral spreading was observed with background pressures above 40 bar. The research concluded that high fuel-injection pressure, small injector hole diameter, optimum fuel viscosity, and high background air pressure are variables to consider towards acquiring suitable fuel spray atomization [4].

1.4 Research Objectives

In this work, multiple control parameters on DME, n-butanol, and diesel fuel injections are investigated empirically. The results of optical observations are analyzed to demonstrate the independent impact of the injection parameter, i.e. injection pressure and background pressure and temperature, on spray characteristics and fuel behaviour. The research efforts

presented in this thesis aim to analyze and compare the spray characteristics of different fuels. Specific research objectives are as follows:

- Analyze the spray characteristics of DME fuel injection at high-pressures.

- Analyze the spray characteristics of diesel and n-butanol fuel injection. By comparing DME fuel spray characteristics with that of other well-known CI fuels, it becomes possible to distinguish the applicability of DME fuel for engines in similar applications.

- Offer a spray characteristics database of DME fuel injection. Understanding the spray characteristics and the behaviour of DME is valuable information to prepare for DME DI research in a single-cylinder research engine (SCRE).

1.5 Thesis Outline

The thesis consists of five chapters. To begin, Chapter I provides the research background, associated challenges, and a review of relevant literature. The main objectives of this research are outlined in this chapter. Chapter II establishes the experimental setups used for the tests. This includes the different tools, methodologies, and processing procedures used to acquire the detailed results in Chapters III and IV. Two experimental approaches are used to analyze the fuel spray, direct imaging and shadowgraph imaging. In Chapter III, DME fuel spray results are discussed, in which the spray penetration length, spray cone angle, and vaporization behaviours are analyzed. In the following chapter, Chapter IV, n-butanol and diesel fuel are subjected to identical testing conditions as DME fuel, and the results are presented, alongside those of DME. The fifth chapter provides a summary of the research outcomes, conclusions, and future work. Further information regarding references, appendices, and a list of publications is provided at the end.

CHAPTER II

EXPERIMENTAL SETUP

The research tools and methodologies used in this study are described in this chapter. Two optically accessible test chambers are used to study spray characteristics of fuel injection under various operating conditions. This information is valuable to expand knowledge for the implementation of any fuel in compression ignition engines.

2.1 Testing Outline

The primary goal of this study is to observe the impacts of parameters including injection pressure, background pressure, and background temperature on the DME spray characteristics and atomization behaviour. Figure 2.1 outlines the general test methodology of this study.
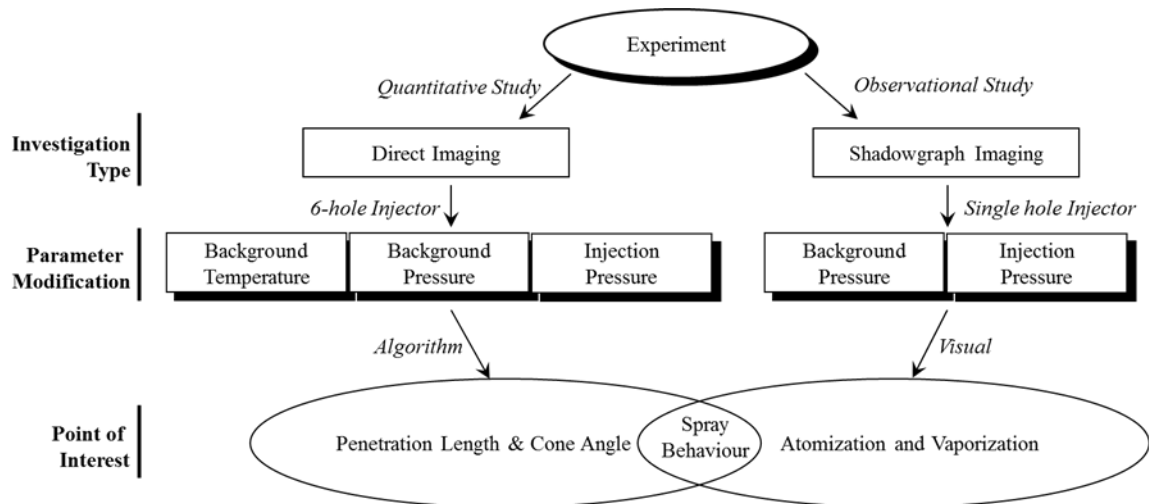
Figure 2.1 The general test methodology

The direct imaging and shadowgraph imaging methods are conducted using a high-speed camera to study the fuel spray atomization process. The direct imaging technique is employed to record the fuel injection process and measure the spray penetration and cone angle through an in-house designed algorithm. In these tests, the fuel spray penetrates through stagnant ambient gas when it is injected into a 2.95L constant-volume chamber through a 6-hole injector. In addition to that, the shadowgraph imaging technique is exclusively used as an observational study. It is employed to observe the transient density changes caused by the fuel spray in a 2.6 L constant-volume chamber (CVC). Testing conditions in this study are presented in Table 2.1.

Table 2.1 Summary of testing conditions

Investigation type	Direct Imaging	Shadowgraph Imaging
Injection duration [μs]	500, 1000	500
Injection pressure [bar]	450, 600, 900	600, 900
Background pressure [bar abs.]	1, 31, 51	1, 11, 21, 31
Background temperature [°C]	30, 110	30

2.2 Experiments

In this work, all high-speed video recordings are separated into individual images and analyzed according to the investigation type. For the quantitative study, the images are processed through a custom algorithm whereas, for the observational study, the images are visually examined. The high-speed camera settings are noted in Table 2.2. The nominal resolution represents the length covered by a single pixel and is used for processing the direct images. Nitrogen (N_2) is the background gas for both investigation types.

13

Table 2.2 Camera settings

Investigation type	Direct Imaging	Shadowgraph Imaging
Frequency [fps]	16000	64000
Exposure time [us]	4	4
Resolution [mm]	512×512	256×128
Nominal resolution [mm/pix]	~0.174	-

In both investigations, the injector and camera triggers are commanded with the aid of an in-house designed LabVIEW program. The command signal is supplied to the Injector Power Driver (IPoD) (EFS 8370) by a field-programmable gate array (FPGA) module (NI PXI-7833R), which is directed by a National Instrument real-time (RT) (NI PXI-8106) controller.

2.2.1 Quantitative Study-Direct Imaging

The overall experimental setup for direct imaging is shown in Figure 2.2. An insulated CVC with three accessible windows is used, as shown in Figure 2.3 alongside the specifications in Table 2.3. This chamber is heated by six cartridge heaters (total 6 kW) installed into the chamber body. A heating unit supplies the energy to these metal cartridges for heating. The temperature is set by the user and controlled by a PID controller in the control unit. As the temperature of the CVC walls rise, so does the temperature of the stagnant ambient gas inside the CVC. Two thermocouples are installed inside the chamber and chamber walls to measure the background gas temperature and wall temperature, respectively. The background pressure is controlled by pneumatic intake and exhaust valves. Compressed air is used to purge the chamber between tests, while N_2 is used as the

background gas for all injection tests. To properly investigate the impacts of background temperature on the fuel spray, the background gas densities should be similar. To accomplish this, the background pressure is initially elevated to the desired amount, followed by increasing the chamber temperature until the background gas reaches the desired temperature. Although the background gas pressure increases from 50 to 64 bar absolute after an increase in temperature, the initial pressure is considered the condition for comparisons.

Figure 2.2 Direct imaging test layout

For this current setup, a diesel piezoelectric injector with six holes (Figure 2.4), each with a diameter of 130 µm, is fitted in the chamber wall facing opposite to the camera viewpoint. The central axes of the injector, the optical window, and the high-speed camera are all aligned. To negate plausible measurement variations during the image processing via the nominal resolution, the distance from the camera flange to chamber face is fixed to 835 mm for all tests, as exemplified in Figure 2.5.
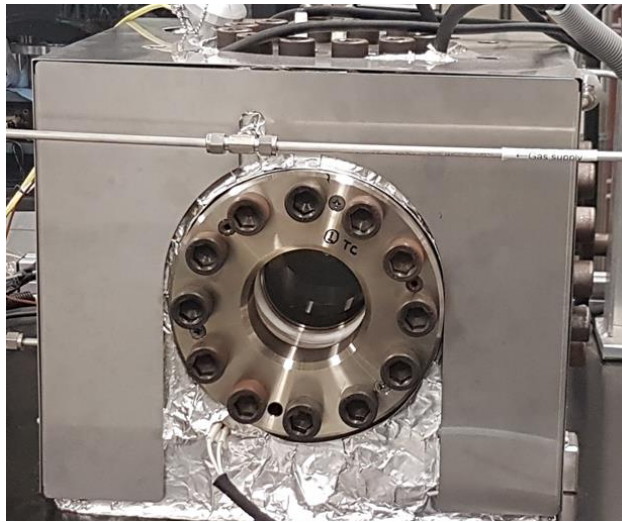
Figure 2.3 Direct imaging CVC

Table 2.3 Direct imaging chamber specifications

Injector	6-hole piezoelectric (130 µm dia.)
Chamber material	Stainless steel SS 304
Dimension [mm^3]	$312 \times 312 \times 305$
Inside volume [L]	2.95
Maximum operating pressure [bar]	150
Maximum operating temperature [°C]	200
Optical window diameter [mm]	110
Optical access diameter [mm]	90
Light source	Halogen

16

Figure 2.4 6-hole piezoelectric injector
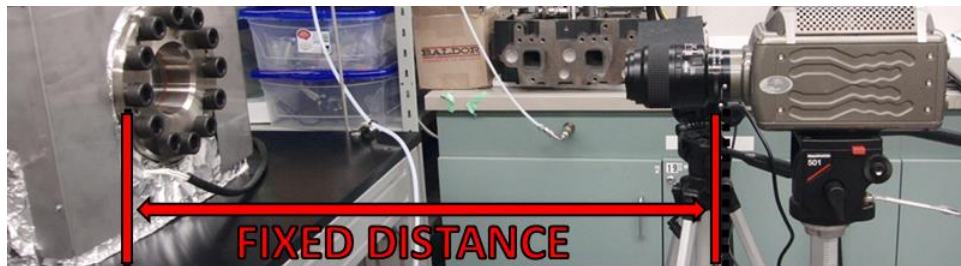
Figure 2.5 High-speed camera setup

2.2.2 Observational Study-Shadowgraph Imaging

The overall experimental setup of the shadowgraph imaging technique is shown in Figure 2.6Figure 2.2. This setup consists of two parabolic optical mirrors, an LED light source, a CVC, and a high-speed camera. The CVC, as shown in Figure 2.7, has a total volume of 2.6 L and three optical windows, with an optical access diameter of 80 mm. A list of the specifications is presented in Table 2.4.

Shadowgraph imaging is a common technique to enhance the visual appearance of fluid vaporization. In general, the premise of shadowgraph imaging is density gradients. As the fuel spray vaporizes and changes state from a liquid to a gas, the density of the fuel will reduce and, in turn, vary the refractive index of the fuel particles. In doing so, the LED light beams that pass through the fuel will refract different amounts of light depending on

17

the state of the fluid, hence visually depicting the phase changes occurring throughout the injection process. The background pressure in the CVC is controlled by pneumatic solenoid valves.
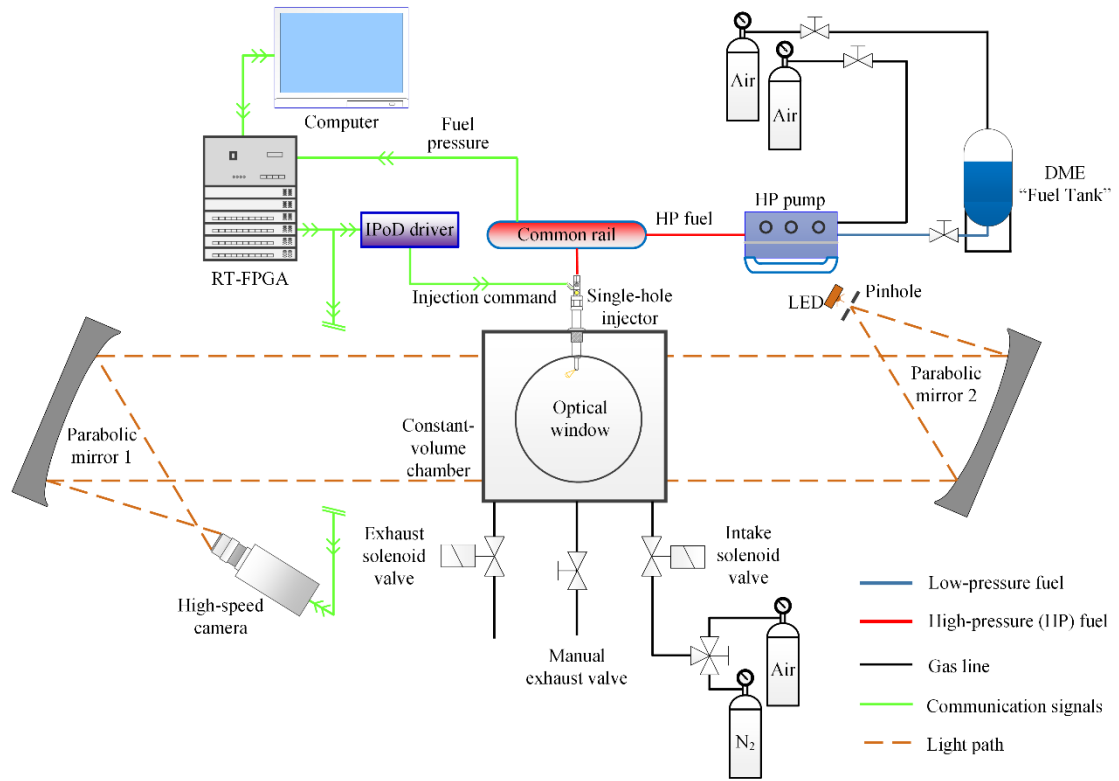
Figure 2.6 Shadowgraph imaging test layout
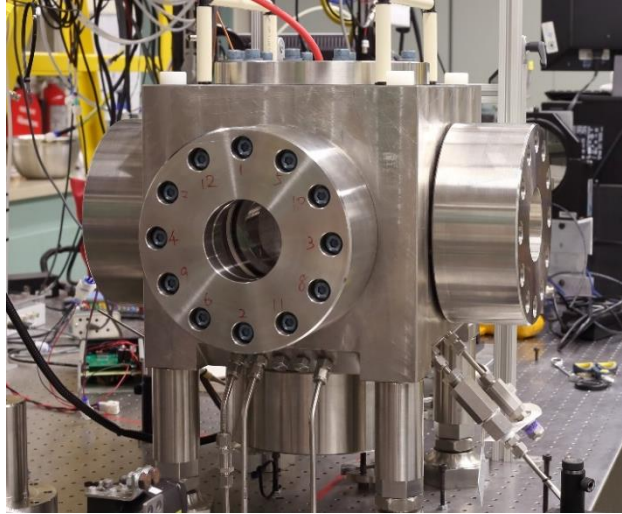
Figure 2.7. Shadowgraph imaging CVC

Table 2.4 Shadowgraph imaging chamber specifications

Injector	1-hole piezoelectric (130 µm dia.)
Chamber material	Stainless steel SS 304
Dimension [mm^3]	$300 \times 300 \times 300$
Inside volume [L]	2.6
Maximum operating pressure [bar]	200
Optical window diameter [mm]	120
Optical access diameter [mm]	80
Light source	LED

To minimize spray interference among multiple plumes during the injection process, a single-hole piezoelectric injector is used for the shadowgraph imaging experiments. This injector is fabricated from an identical injector that used in the direct imaging experiments. The injector is modified by laser welding five of the six 130 µm injector nozzle holes. This injector, as shown in Figure 2.8, is used for all the shadowgraph imaging tests. The injector is mounted at the top of the chamber, wherein the single-hole spray is aimed normal to the camera viewpoint.

Figure 2.8 Single-hole piezoelectric injector

2.3 Fueling System

Suitable fuel handling is important to safely implement dimethyl ether (DME) in an engine. The DME fueling system used in this work is configured to achieve two primary goals: (1) to fill the portable DME fuel tank; and (2) to supply high-pressure fuel for injection. The procedure to achieve these goals is described below.

(1) To fill the portable DME fuel tank

A large stand-still supply tank is used to store a large amount of DME, while a 1-gallon portable tank is used for the investigations. To fill this portable tank, a secure connection must first be made between the large DME supply tank and the bottom of the portable DME fuel tank. The top and bottom are instrumented with a 3-way fitting. When filling the portable tank, the angle stop valve of the supply tank should be fully open. To begin, slightly open the top of the portable tank to allow the release of pressure, and finally open the bottom connection to allow DME fuel from the supply tank to flow. While the fuel tank

is filling, it is important to be attentive during the process and prepared to immediately close the supply tank valve in case of an emergency. Once DME fuel, a white gaseous substance, releases through the pressure relief, the portable tank is filled. Shut off the supply tank valve and the 3-way fitting at the bottom of the fuel tank.
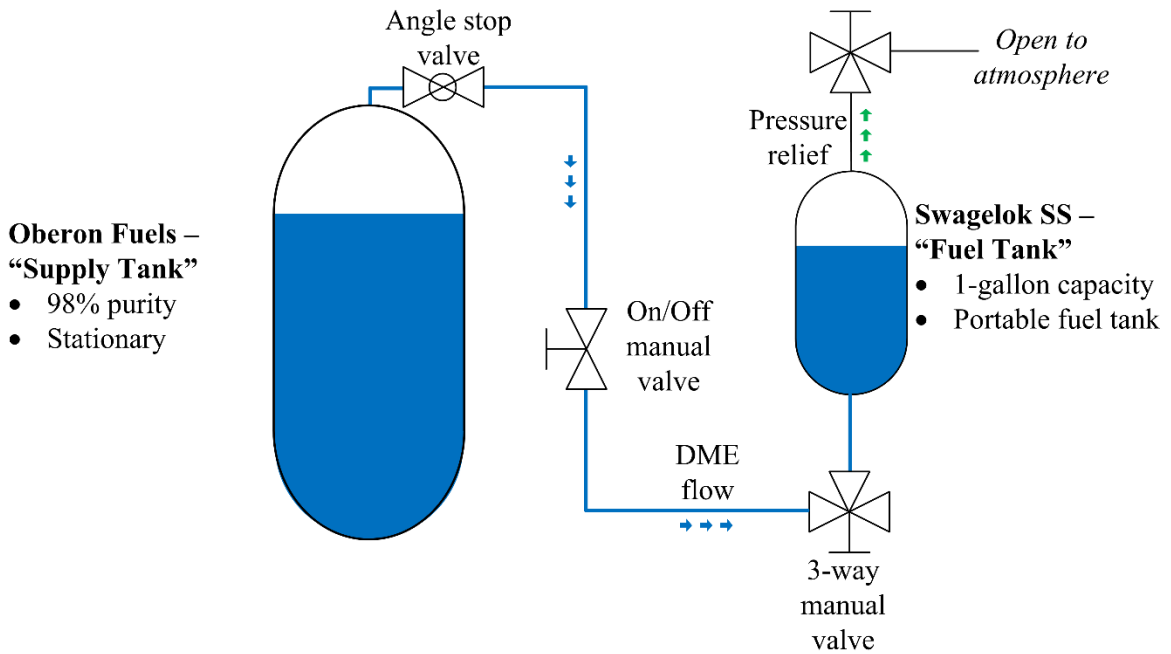
Figure 2.9 Fuel filling system schematic

(2) To supply high-pressure fuel for injection

The DME fuel injection system used for the experiments is shown in Figure 2.10. It contains four principal parts: a dry-compressed air tank, a portable fuel tank, a high-pressure liquid pump, and a diesel common rail. Among these parts, three secure connections are made: (1) between the bottom of the portable DME fuel tank and the high-pressure (HP) pump, (2) between the compressed dry-air tank and the top of the portable DME fuel tank, and (3) between the compressed dry-air tank and the driving air connection for the HP pump. The portable DME fuel tank is pressurized up to 7 bar absolute pressure

21

by compressed dry-air. This elevated pressure ensures that liquid DME will be supplied to the pump. The fuel injection pressure is achieved by managing the inlet pressure regulator of the pump.

The pump utilized in this work is a Maximator LSF100-2 pneumatic pump. It consists of a single-acting pump with a double air drive head, sealed with Viton O-rings (a DME-safe material). The inlet to outlet pressure ratio of the pump is 1:226 and has a maximum outlet pressure rating of 1600 bar. A sufficient amount of time is given for the pump to stabilize the pressure at the desired outlet value. A diesel common-rail is installed as an intermediate stage to aid the stabilization of the fuel pressure.
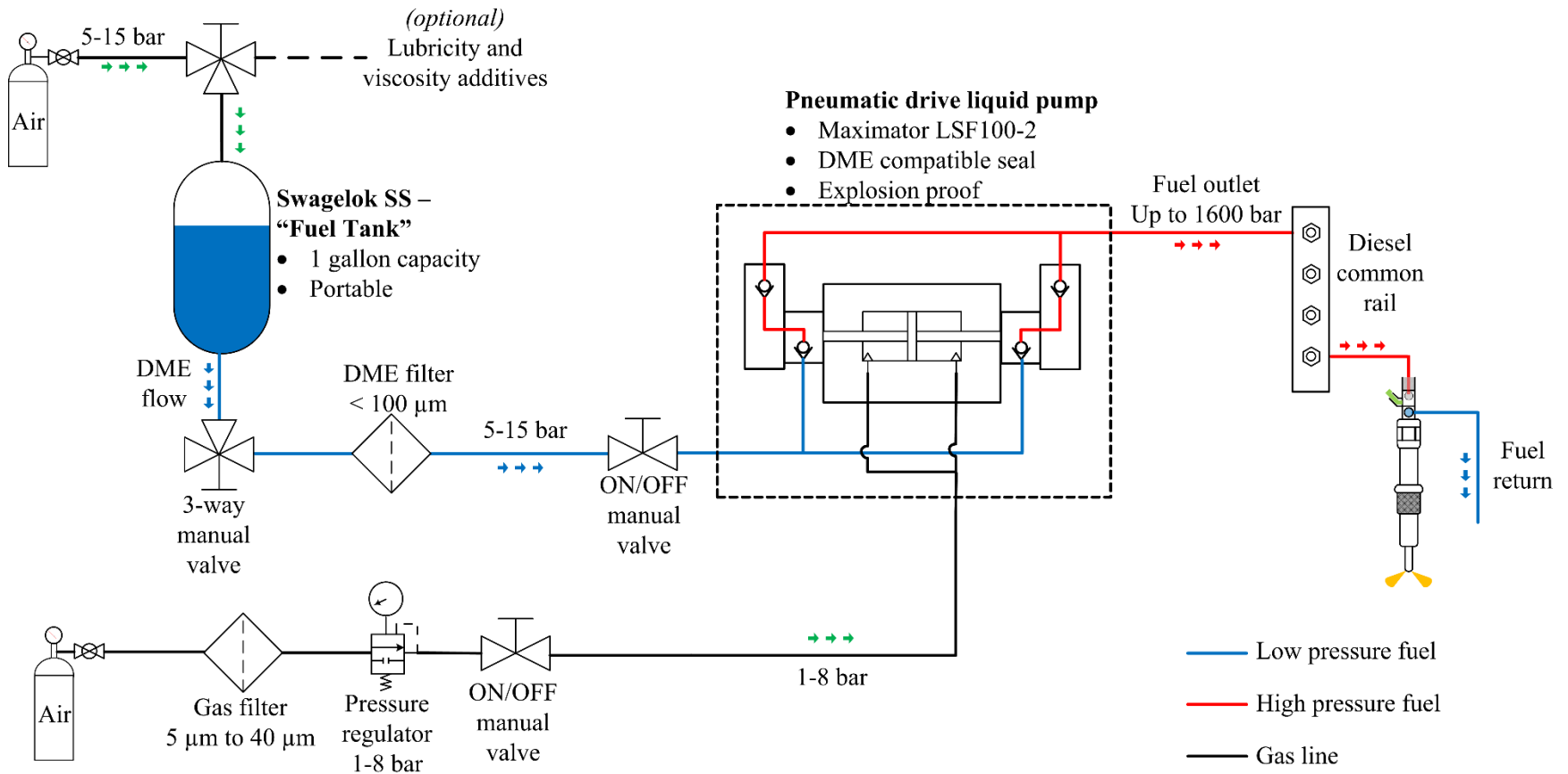
Figure 2.10 Fuel handling system layout

2.4 Processing Algorithm

To minimize human error through manual measurement, all the direct imaging experiment recordings are processed with the same algorithm. A single injection plume is chosen as the spray of interest for all the data tests. A general outline of the observed spray characteristics is shown in Figure 2.11. The analysis of the test data is done using an in-house designed code, presented in APPENDIX A. This code is designed to import individual images, isolate the plume of interest, and output the resulting spray penetration length and cone angle. The pixel intensity threshold of 5 is held constant through each analysis. Pixels value with an intensity level above the threshold is defined as the liquid spray region and used for processing, whereas pixels less than the intensity threshold are deemed as insignificant, i.e. possible light reflection.
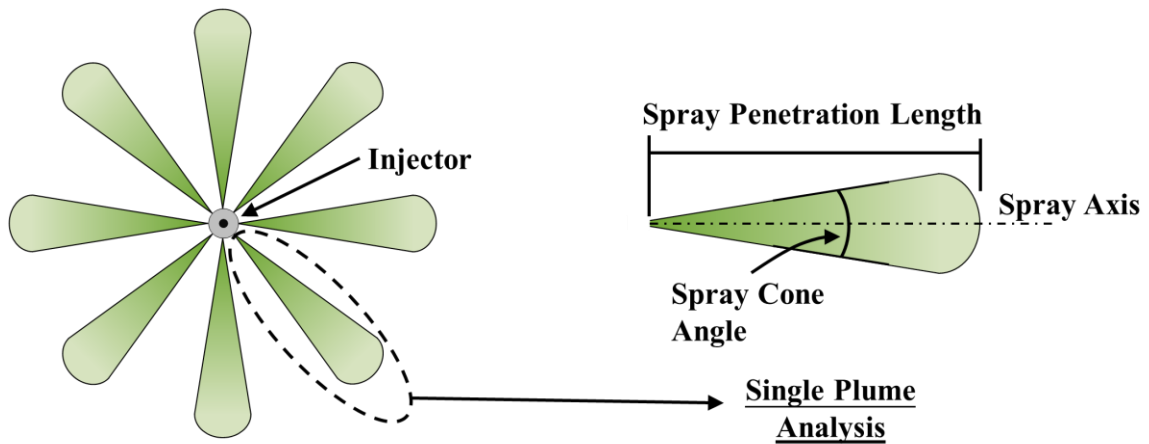
Figure 2.11 Fuel injection spray characteristics

The spray axis is manually defined by the user in the algorithm and the first pixel located along on that axis defines the injector nozzle hole. The spray penetration length is defined as the maximum distance the fuel reaches, along the spray axis [56]. The spray cone angle

of the outer boundary of a spray is a common measure of spray dispersion [64]. Since the

spray boundaries are curved, a definition for spray cone angle is difficult to generalize [56].

In this work, the spray cone angle is measured by the angle resulting from a linear

regression fitted line of the spray body boundary, i.e. 25-75% of the spray penetration

length, intersecting through the injector nozzle hole. Figure 2.12 illustrates this measuring

technique. Most spray characteristic results presented in this thesis are based on an average

of six identical test cases.
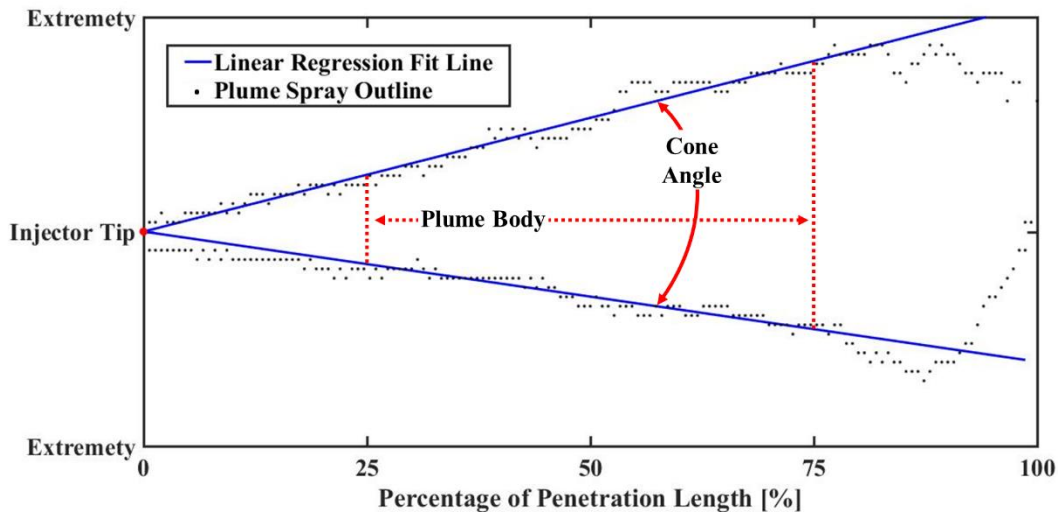
Figure 2.12 Algorithm measuring techniques

2.5 Summary

In this work, an empirical study is undertaken to describe the spray characteristics of DME.

The spray penetration length and cone angle formed throughout the fuel injection process

is studied using a 6-hole piezoelectric injector and a direct imaging technique. The

vaporization behaviour of DME fuel is studied using a single-hole injector and a

shadowgraph imaging technique. The results are compared to well-established fuels used

in DI CI engines, n-butanol and diesel.

CHAPTER III

SPRAY CHARACTERISTICS OF DME

The fuel spray characteristics and spray quality are important factors in direct injection (DI) compression ignition (CI) engine applications. The spray penetration length, spray cone angle, and atomization behaviour can help determine the suitability of a fuel in DI CI engine applications. In this chapter, the fuel spray behaviour is studied using direct imaging and shadowgraph imaging techniques. The images obtained by the direct imaging technique are used to measure spray characteristics, such as spray penetration length and cone angle. The shadowgraph imaging is employed to observe the density differences through light refraction [65]. The technique is used to capture the vaporization of the fuel within the fuel injection process. Throughout the experiments, each parameter is independently controlled to investigate its impact on the fuel spray characteristics. The parameters tested include injection pressure, background pressure, and background temperature.

3.1 Spray Penetration Length and Cone Angle

The injection tests are conducted to study the effect of the injection pressure, background pressure, and background temperature on the fuel spray characteristics of dimethyl ether (DME). During the injection process, a high-speed camera is used to record the fuel spray from the start of injection (SOI) until the end of injection (EOI).

3.1.1 Injection Pressure

For this study, the injection pressures of 450, 600, and 900 bar are selected. The background pressure is kept at 1 bar absolute and 500 µs of fuel injection duration is commanded.

The images captured from the high-speed direct imaging tests of DME fuel spray under different injection pressures are shown in Figure 3.1. A faster spray penetration rate is the primary effect observed by increasing the injection pressure.
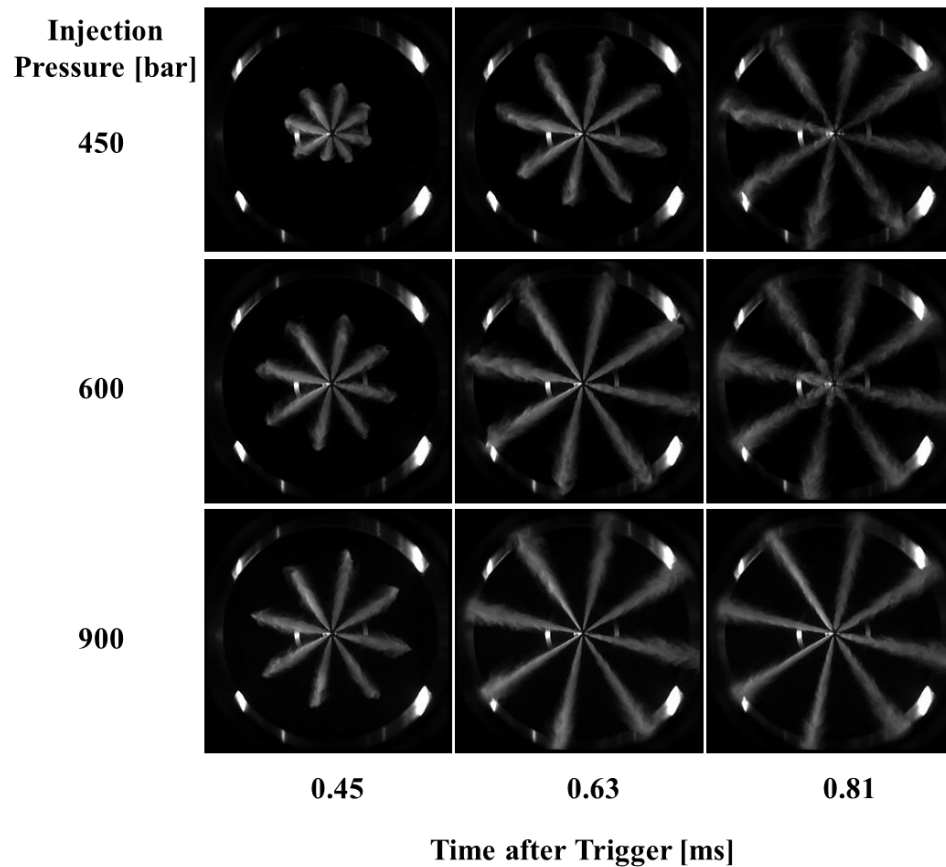
Figure 3.1 Direct fuel spray images of DME at 450, 600, and 900 bar injection pressure and 1 bar absolute background pressure

The data presented in Figure 3.2 (a) and (b) depict the measured spray penetration lengths and spray cone angles, respectively. It is clear that the spray penetration length increases with the injection pressure values. This can be understood with the Bernoulli's relation. The principle in Equation 3.1 [66] shows that the exit velocity of a fluid increases with a larger difference in fuel pressure and background gas pressure. In these cases, the spray tip velocities follow a similar trend. At 0.45 ms after the trigger, injection pressures of 450, 600, and 900 bar exhibit an approximate spray tip velocity of 48, 85, and 130 mm/s, respectively. During the initial development of the fuel sprays, relatively wide cone angles are observed, ranging from approximately 80° to 50°. The spray cone angles at the SOI are shortened with an increase of injection pressure. Additionally, the time taken to reach the steady cone angle is reduced with an increase in injection pressure.

$$u_e = \sqrt{\frac{2 \cdot \Delta p}{\rho_f}} \qquad\qquad 3.1$$

Where,

Δp	the difference between fuel and background gas pressure	[kPa]
u_e	the exit velocity of the fuel	[m/s]
ρ_f	the fuel density	[kg/m³]
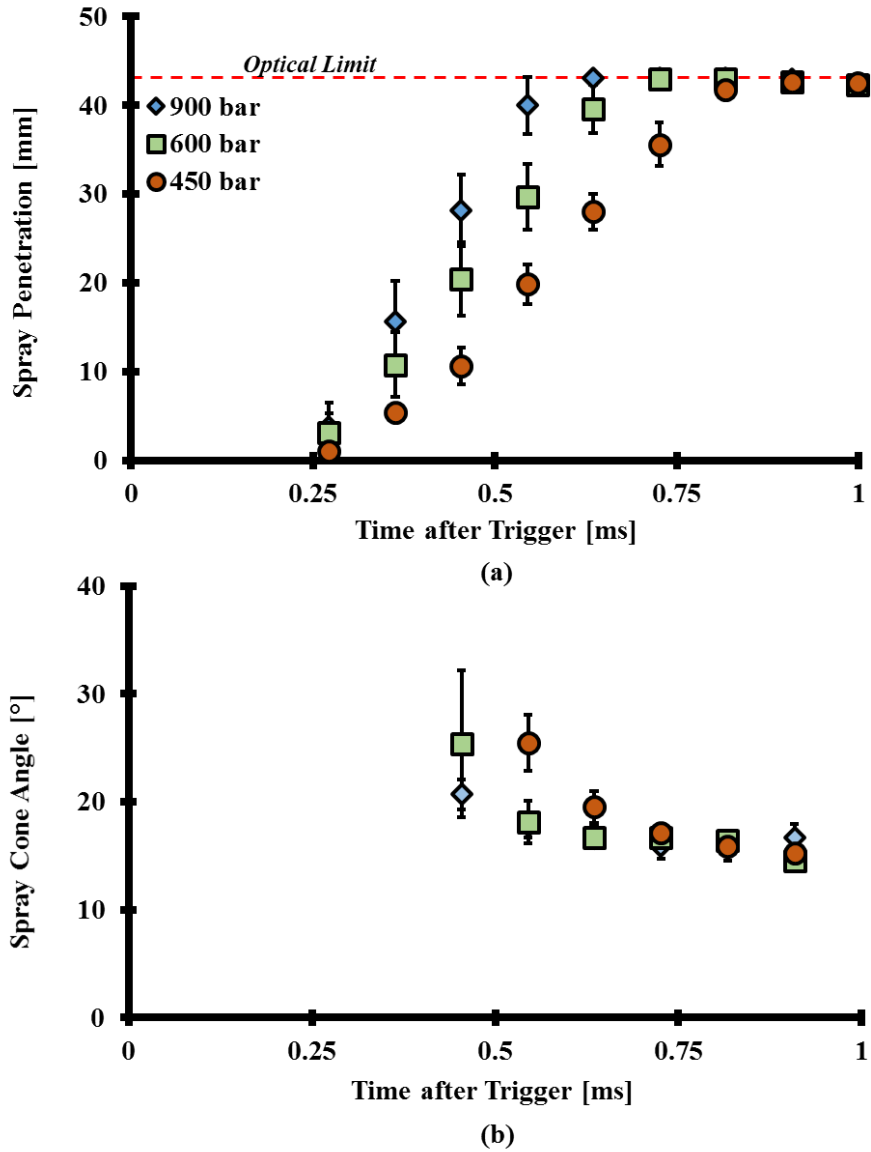
Figure 3.2 Spray characteristics of DME at 450, 600, and 900 bar injection pressure and 1 bar absolute background pressure

Further testing involves a higher background pressure of 51 bar absolute under the same injection pressures, shown in Figure 3.3. Similar to previous conclusions, the primary impact of injection pressure is observed on the spray penetration length.

29
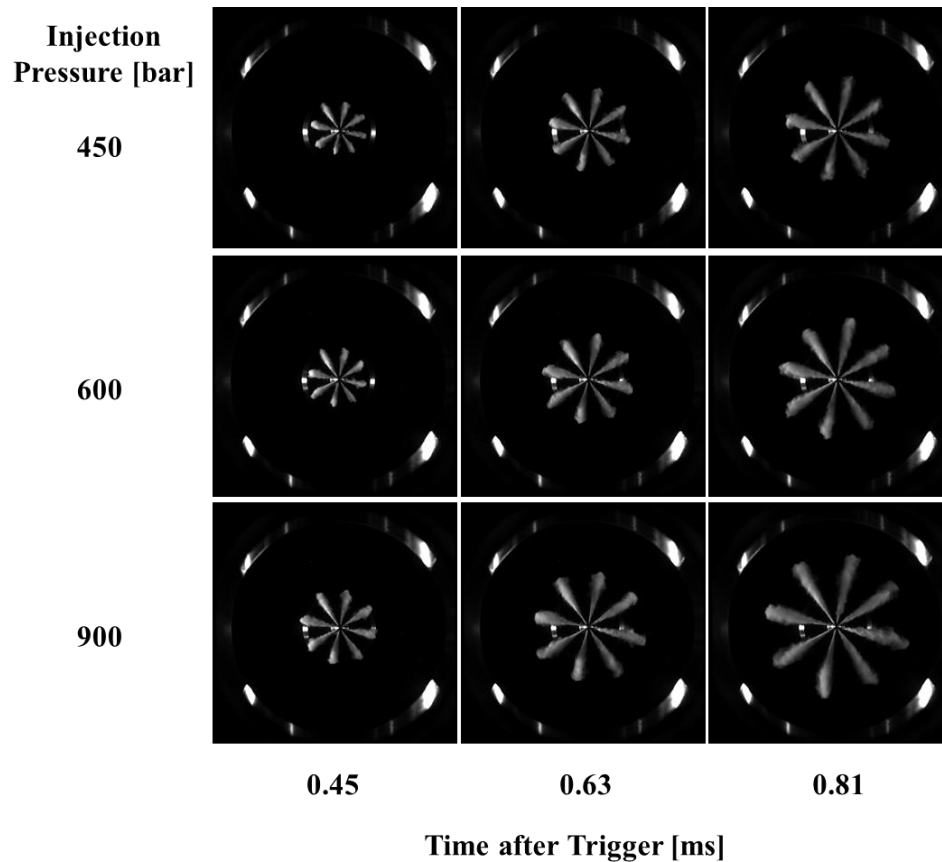
Figure 3.3 Direct fuel spray images of DME at 450, 600, and 900 bar injection pressure and 51 bar absolute background pressure

The corresponding spray penetration lengths are shown in Figure 3.4 (a). Under 51 bar absolute background pressure, the spray penetration lengths vary by less than 5%. Due to measurement uncertainty being high until 0.45 ms after the trigger, high variations are expected. Beyond this uncertainty, the spray tip velocities range within 8 mm/s of each other until 1.63 ms after the trigger. Moreover, the spray cone angles of each condition exhibit a peak coefficient of variation (COV) of 15% until 1.27 ms after the trigger, as shown in Figure 3.4 (b). Due to the marginal differences in the spray cone angle among these cases, it is concluded that the injection pressure has no impact on the spray cone angle.

(a)

(b)
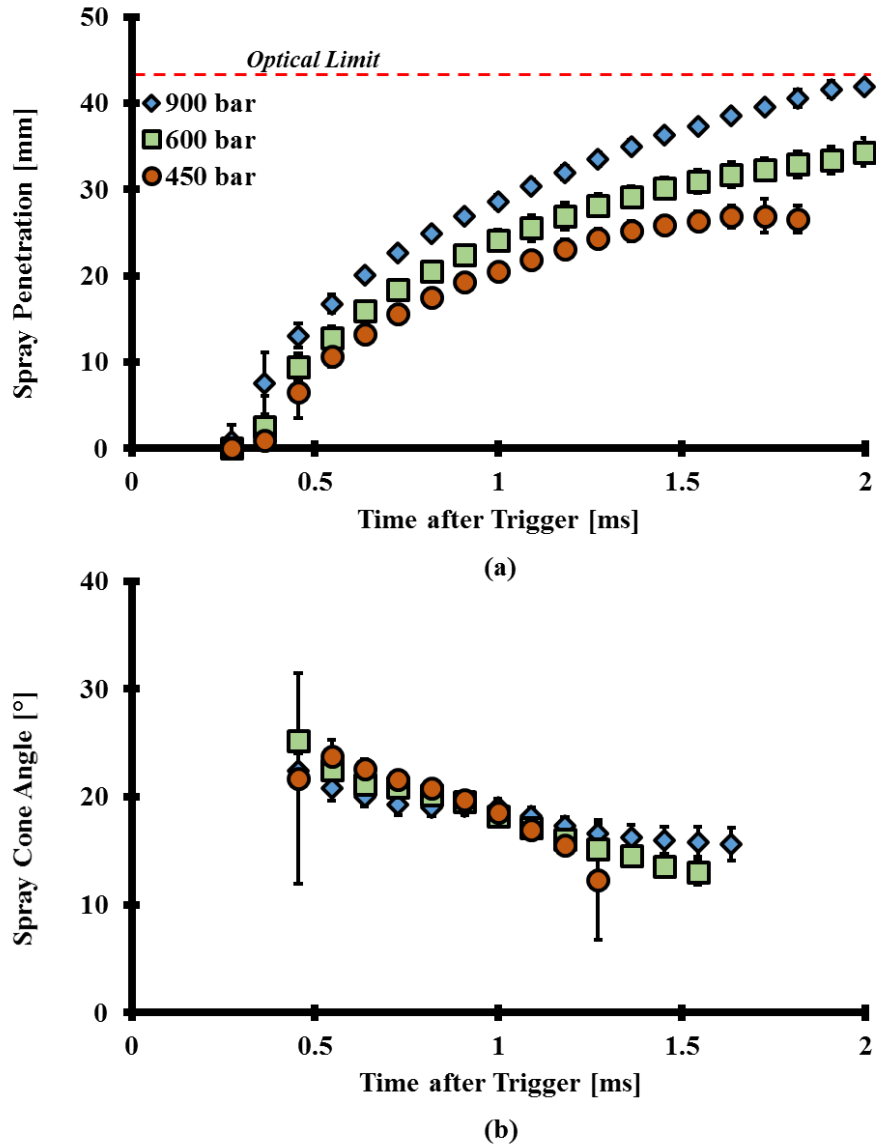
Figure 3.4 Spray characteristics of DME at 450, 600, and 900 bar injection pressure and 51 bar absolute background pressure

3.1.2 Background Pressure

The impact of 1, 31, and 51 bar absolute background pressures on the spray characteristics of DME fuel spray are investigated in this section. An injection duration command of 500 µs is kept constant throughout the tests. The spray images of DME fuel at 450 bar injection pressure into various background pressures are shown in Figure 3.5. The change in

background pressure strongly affects the background gas density, a key parameter that affects the spray characteristics [64,67]. The reduction in spray penetration length is best described in a publication by Naber and Siebers [64], wherein the authors describe "as ambient gas density increases, spray dispersion increases, which results in more entrained air in the spray. The larger entrained mass leads to a slower penetration velocity based on conservation of momentum, and therefore, reduced penetration."
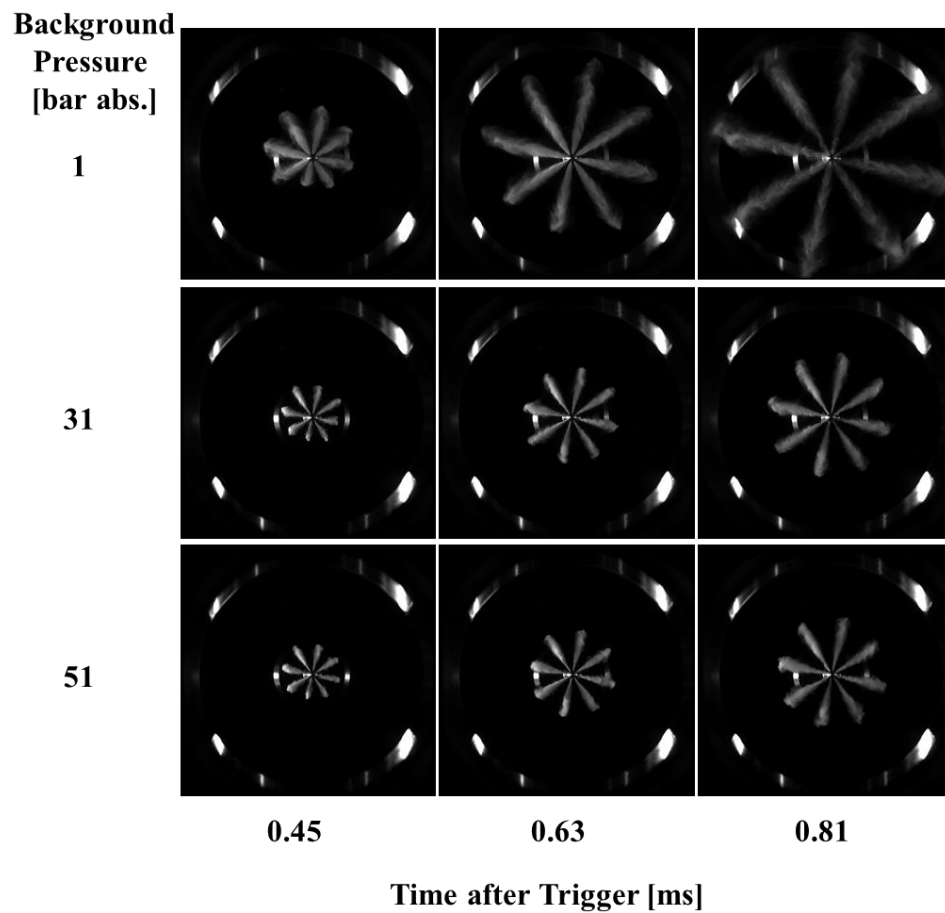
Figure 3.5 Direct fuel spray images of DME at 450 bar injection pressure and 1, 31, and 51 bar absolute background pressure

In Figure 3.6, it is observed that the DME spray demonstrates similar traits as the background pressure increases. Because the background density is proportional to the value of the background pressure, more obvious differences between the spray characteristics are observed when the background pressure is increased from 1 bar to 31 bar absolute than 31 bar to 51 bar absolute.

At 0.81 ms after the trigger, the spray penetration length observed at 31 bar absolute background pressure is around 50% of the spray penetration length observed when the background pressure is 1 bar absolute. On the other hand, an increase in background pressure from 31 to 51 bar absolute leads to a decrease of 14% in the length of spray penetration. At the same time, the spray cone angle observed at 31 bar absolute background pressure is nearly 25% wider than the fuel spray is subjected to 1 bar absolute background pressure. A further 6% increase in the spray cone angle is observed from 31 to 51 bar absolute background pressure.
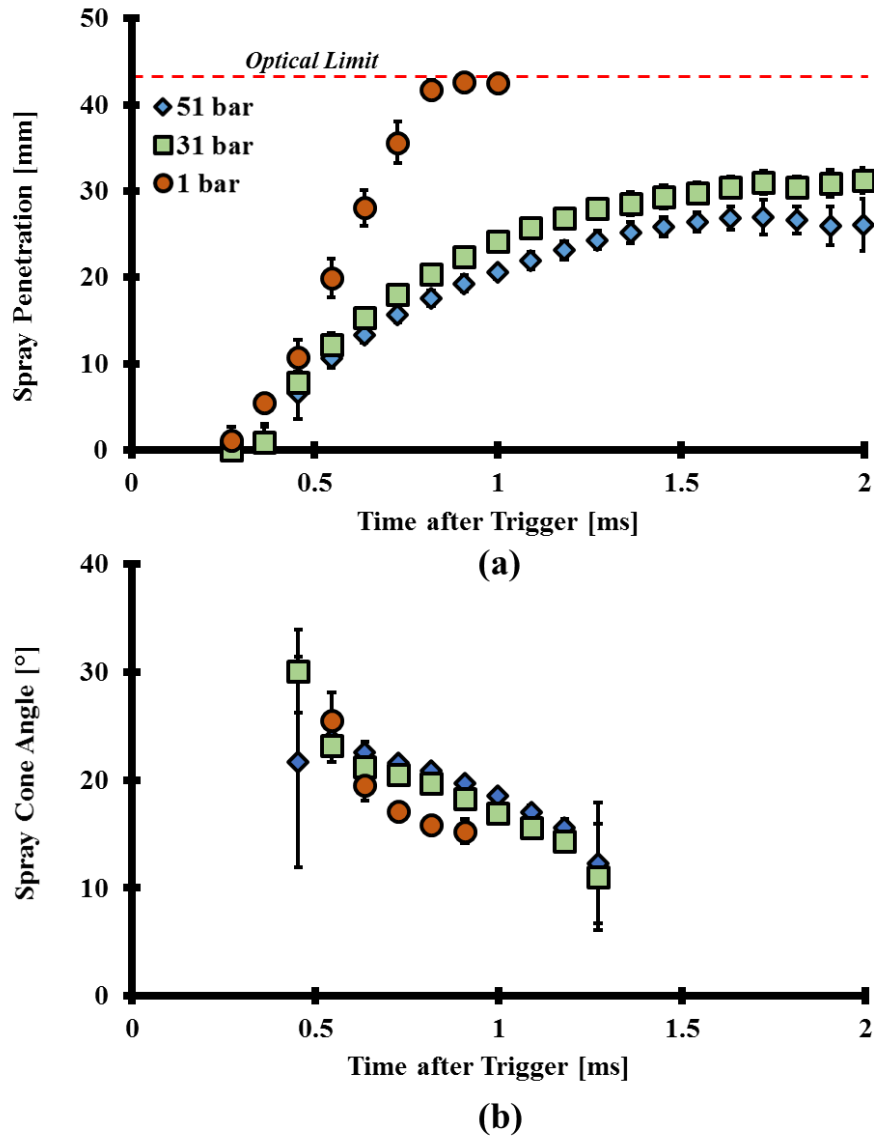
Figure 3.6 Spray characteristics of DME at 450 bar injection pressure and 1, 31, and 51 bar absolute background pressure

The DME fuel spray images shown in Figure 3.7 are subjected to an injection pressure of 900 bar and background pressure values of 1, 31, and 51 bar absolute. As concluded previously in Figure 3.6, the spray penetration length decreases with an increase of background pressure values.
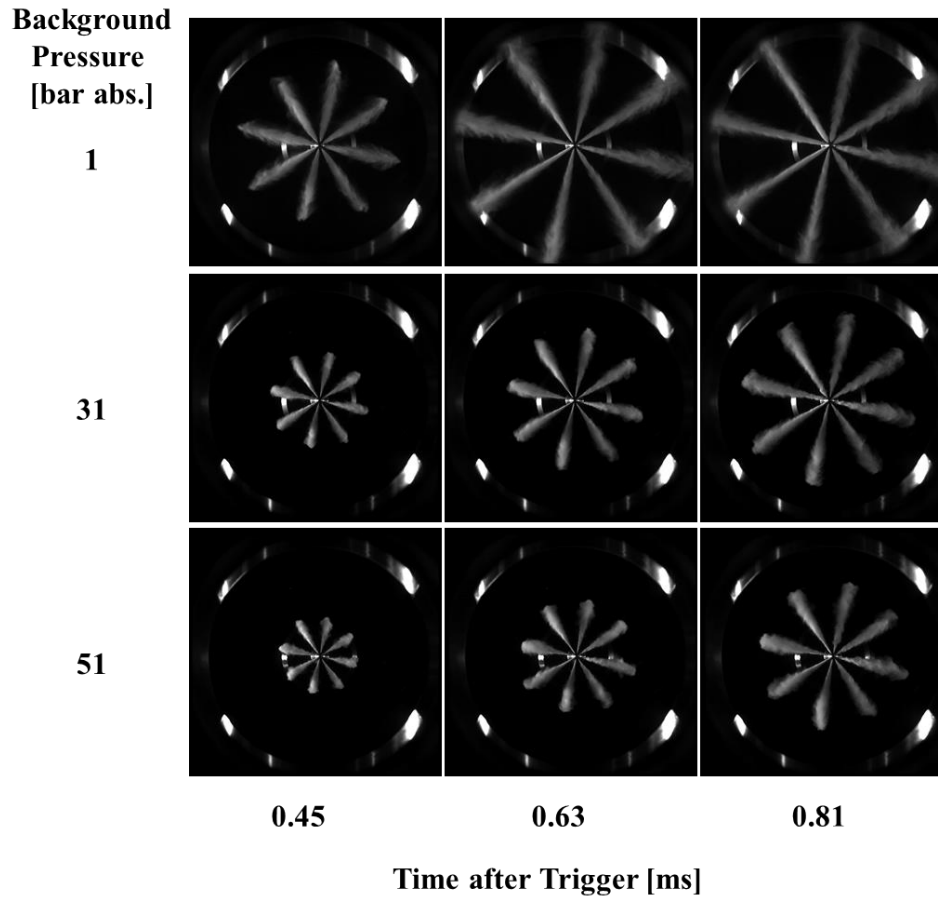
Figure 3.7 Direct fuel spray images of DME at 900 bar injection pressure and 1, 31, and 51 bar absolute background pressure

DME fuel evaporates the fastest under 1 bar absolute background pressure. This is because the background pressure is lower than the saturation vapour pressure of DME (~6 bar absolute). In Figure 3.8 (a), at 0.36 ms, the standard deviation in spray penetration length reduces from 4.6 mm to 1.5 mm under 1 and 51 bar absolute, respectively. Under 1 bar absolute background pressure, the peak value for the COV is 29%. On the other hand, a peak COV of 7% and 17% are observed under 31 and 51 bar absolute, respectively. Among the three background pressure conditions, the majority of the spray cone angles lie within a range of 3-4°, as shown in Figure 3.8 (b).
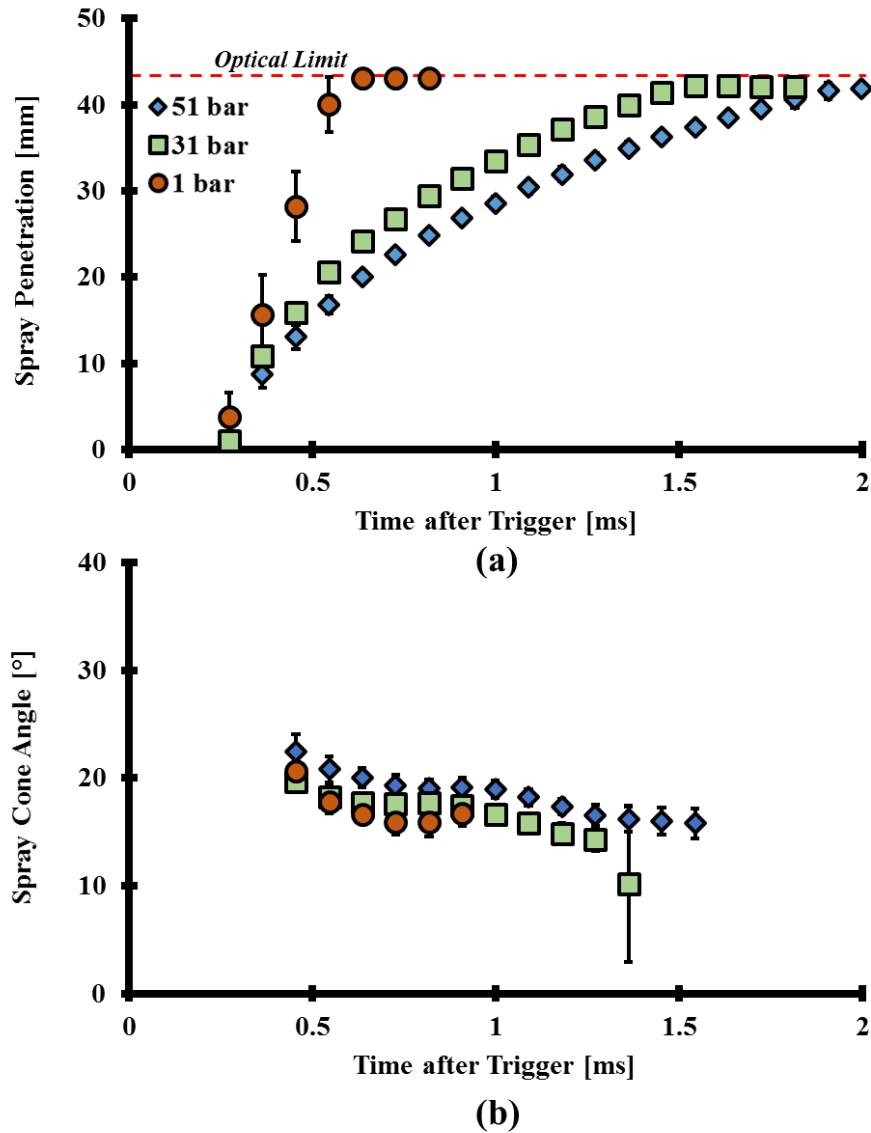
Figure 3.8 Spray characteristics of DME at 900 bar injection pressure and 1, 31, and 51 bar absolute background pressure

3.1.3 Background Temperature

The purpose of this section is to analyze the impact of background temperature on the spray characteristics and behaviour of DME fuel. To maintain a constant background gas density under various temperature conditions, the constant-volume chamber (CVC) that is used for investigating different background temperature conditions is pressurized first and then

heated up to the target temperature. In this work, the injection pressure is kept constant at 600 bar. The spay characteristics of DME are examined under two background temperatures, 30 and 110 °C, each tested under 1 and 51 bar absolute background pressure.

The images obtained from DME fuel spray under 1 bar absolute background pressure are shown in Figure 3.9. When the DME fuel is injected into the chamber, a substantially wide fuel spray is observed once the fuel leaves the injector nozzle. In relation to the phase change characteristics described in Chapter I (Figure 1.2), a flash boiling effect is present under 1 bar absolute background pressure. Comparing with 30 °C background temperature, this effect is more obvious when the background temperature increases, evident by the extremely wide spray cone angle under 110 °C background temperature. The presence of flash boiling affects the spray quality, more specifically, flash boiling leads to finer droplet sizes, wider spray cone angles, and consequently, a shorter spray penetration length [68].
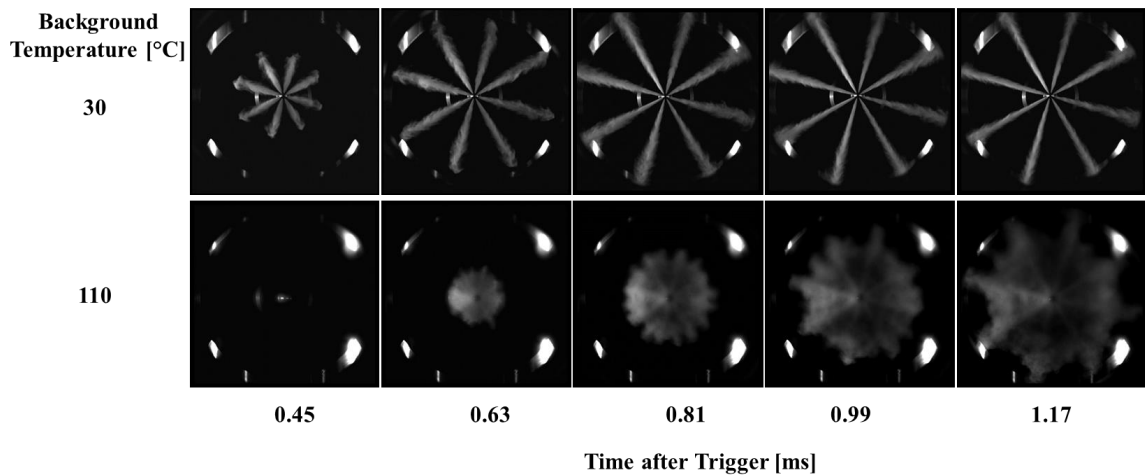
Figure 3.9 Direct fuel spray images of DME at 600 bar injection pressure, 1 bar absolute background pressure, and 30 and 110 °C background temperature

The corresponding spray penetration lengths are presented in Figure 3.10. Two different injection delays are exhibited between the two tested cases, however, the cause is not investigated in this work. To ignore this offset, the data is advanced appropriately so that the SOI for both cases is used as a "reference time" of 0 ms, as shown in Figure 3.10 (b). Because the flash boiling effect causes a wider spray cone angle, an increase in background temperature slightly reduces the spray penetration length.
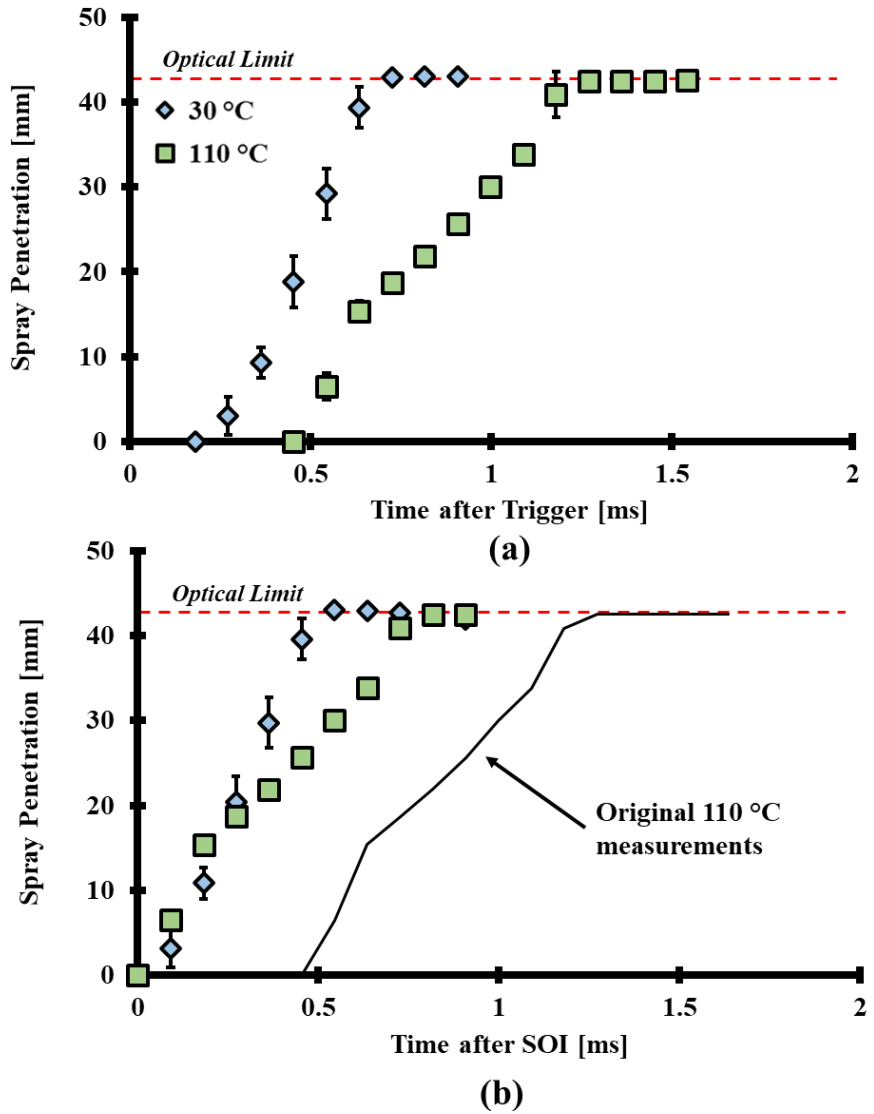
Figure 3.10 Spray characteristics of DME at 600 bar injection pressure, 1 bar absolute background pressure, and 30 and 110 °C background temperature

The images of DME fuel spray into a heated background gas under 51 bar absolute background pressure are shown in Figure 3.11. It is important to note that the background gas densities between the two conditions are identical. The CVC is first pressurized to 51 bar absolute with N_2, followed by increasing the temperature of the stagnant background gas to 110 ℃.
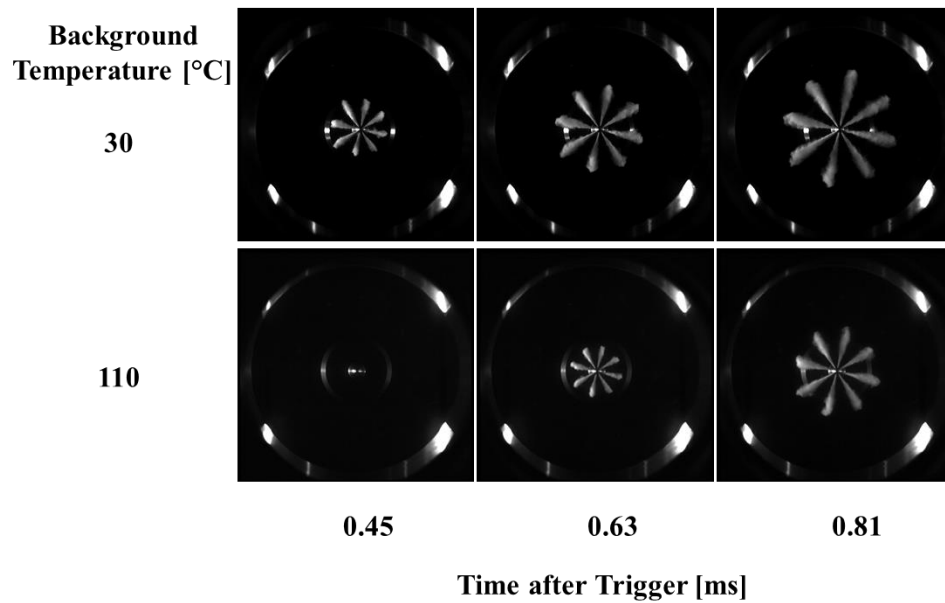
Figure 3.11 Direct fuel spray images of DME at 600 bar injection pressure, 51 bar absolute background pressure, and 30 and 110 ℃ background temperature

The relevant spray characteristics are plotted in Figure 3.12. It can be seen that the increase of the background temperature results in a longer injection delay, from 0.27 ms to 0.45 ms. The following conclusions are assuming simultaneous SOI, similar to the prior data alteration exemplified in Figure 3.10 (b). Beyond 0.27 ms after the SOI, the increase in background temperature causes a maximum of 5% difference between 30 and 110 ℃ in spray penetration length. In regards to the spray cone angle, a higher background

39

temperature causes a larger standard deviation. For example, at 0.63 ms after the SOI, the spray cone angle exhibits a COV of 5% under 30 ℃, whereas a COV of 28% is observed under 110 ℃ background temperature. However, the spray cone angles converge and reach similar steady spray cone angles as the fuel penetrates.
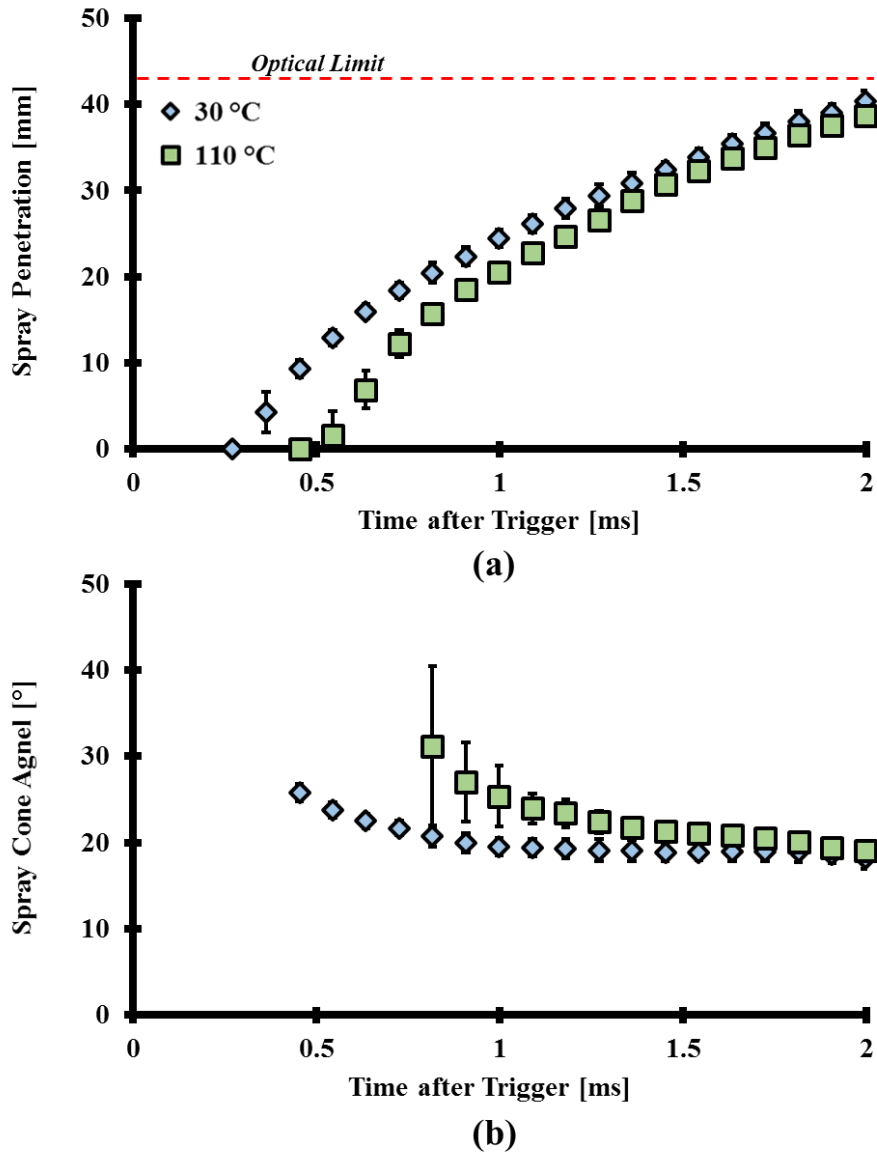
Figure 3.12. Spray characteristics of DME at 600 bar injection pressure, 51 bar absolute background pressure, and 30 and 110 °C background temperature

Under 1 bar absolute pressure, the boiling point of DME is near -25°C [28]. The Clausius-Clapeyron equation models the relationship between the vapour pressure and the boiling temperature of a liquid, as shown in Equation 3.2 [69]. According to this equation, the boiling point of DME fuel is nearing 130°C under 51 bar absolute background pressure. Therefore, flash boiling effects are unlikely to happen under such high background pressures. This is the reason as to why flash boiling is presented in DME spray under 1 bar absolute background pressure, yet not presented under 51 bar absolute background pressure.

$$T_B = \left(\frac{1}{T_0} - \frac{R \cdot \ln\left(\frac{p}{p_0}\right)}{\Delta H_{vap}} \right)^{-1}$$

3.2

Where,

T_B	the boiling temperature	[K]
ΔH_{vap}	the enthalpy of vaporization	[J/mol]
R	the ideal gas constant	[J/mol·K]

Due to the increase in the boiling point of DME fuel, the flash boiling effects observed under elevated background temperature (recall Figure 3.9) are nullified by the increase in background pressure. A lengthened timespan up to 1.17 ms after the trigger for the spray under these two background pressure conditions is shown in Figure 3.13 for comparison.
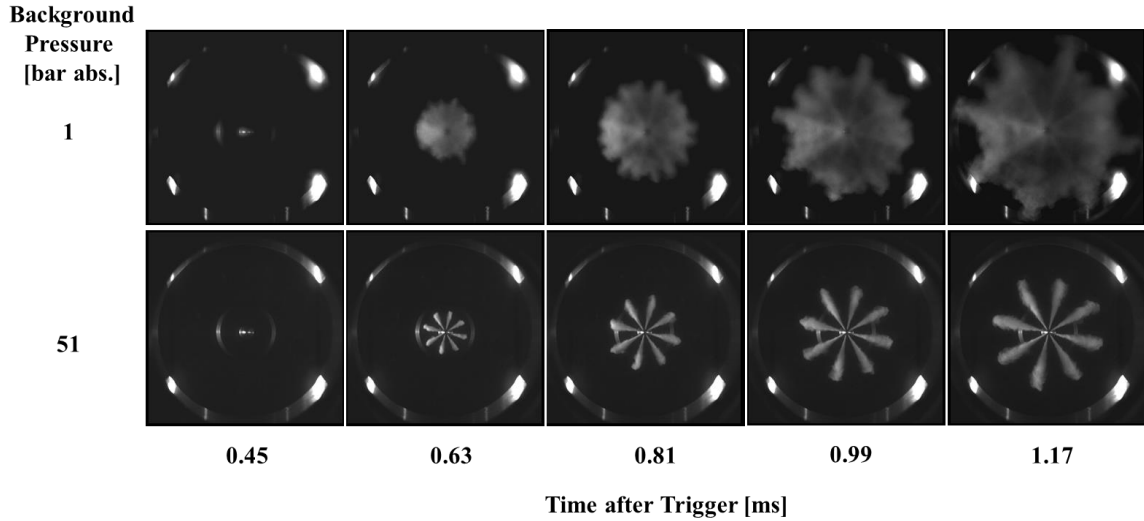
Figure 3.13 Direct fuel spray images of DME at 600 bar injection pressure, 1 and 51 bar absolute background pressure, and 110 °C background temperature

3.2 Vaporization

The prevalent spray characteristics of DME spray have been concluded in Chapter III. The direct images are used to measure the spray penetration length and cone angle which detail the spray behaviour of the liquid DME fuel. The use of shadowgraph imaging provides a visual demonstration of the fluid density changes that take place during the fuel injection process [65]. The density changes are representative of the phase changes occurring, in which a lower density fluid refracts less light. For the images shown in this section, the vaporization is represented by the various shades of black particles surrounding the contour of the fuel spray (black pixels). As the pixels become brighter, the fluid particles are deemed more gaseous.

Insight into this vaporization behaviour is shown in Figure 3.14. At the beginning stage, black particles can be observed exiting the injector nozzle. These black particles represent

the fuel in a liquid phase. As the fuel spray further penetrates, the contour of the plume exhibits particles with a lighter shade of black, detailing the density gradients that are present. Under 1 bar absolute background pressure, the DME fuel spray exhibits increasingly noticeable vaporization as the fuel reaches the extremities of the chamber. While vaporization is mostly observed near the spray tip, some vaporization lingers along the outer edges. Furthermore, an increased vaporization behaviour in the fuel spray is observed with an increase in background pressure.
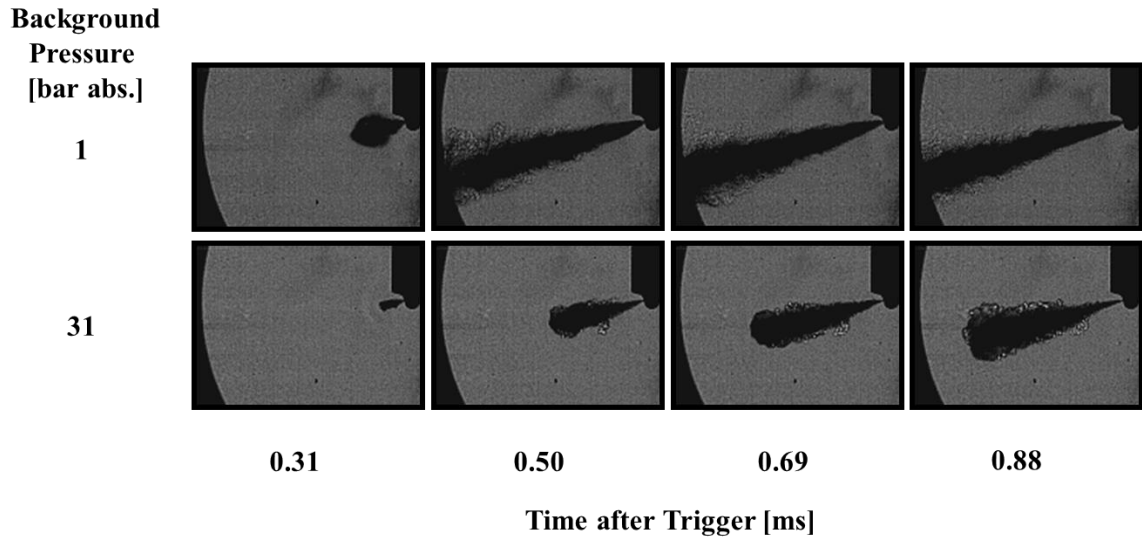
Figure 3.14 Shadowgraph fuel spray images of DME at 600 bar injection pressure, and 1 and 31 bar absolute background pressure

CHAPTER IV

FUEL COMPARISON

The impacts of various injection and background parameters on the spray characteristics of dimethyl ether (DME) are detailed in Chapter III. Therein, the focus includes the spray penetration length, spray cone angle, and the vaporization behaviour of DME fuel throughout the injection process. This chapter presents details on the spray characteristics of two established fuels for compression ignition (CI) engines, diesel and n-butanol. In this manner, comparisons between DME fuel and direct injection (DI) applicable fuels can be realized for consideration in the future implementation of DME fuel in CI engine applications.

4.1 Spray Penetration Length and Cone Angle

In this section, direct imaging experiments are used to compare the spray characteristics of DME, n-butanol, and diesel. This section is split into the two parts, injection pressure and background pressure.

4.1.1 Injection Pressure

Under 1 bar absolute background pressure, it is apparent that the fuels exhibit unique spray behaviours, as shown in Figure 4.1. Diesel fuel presents a fast, sharp, and narrow plume throughout the entire injection process. n-Butanol presents similar spray characteristics to diesel fuel.
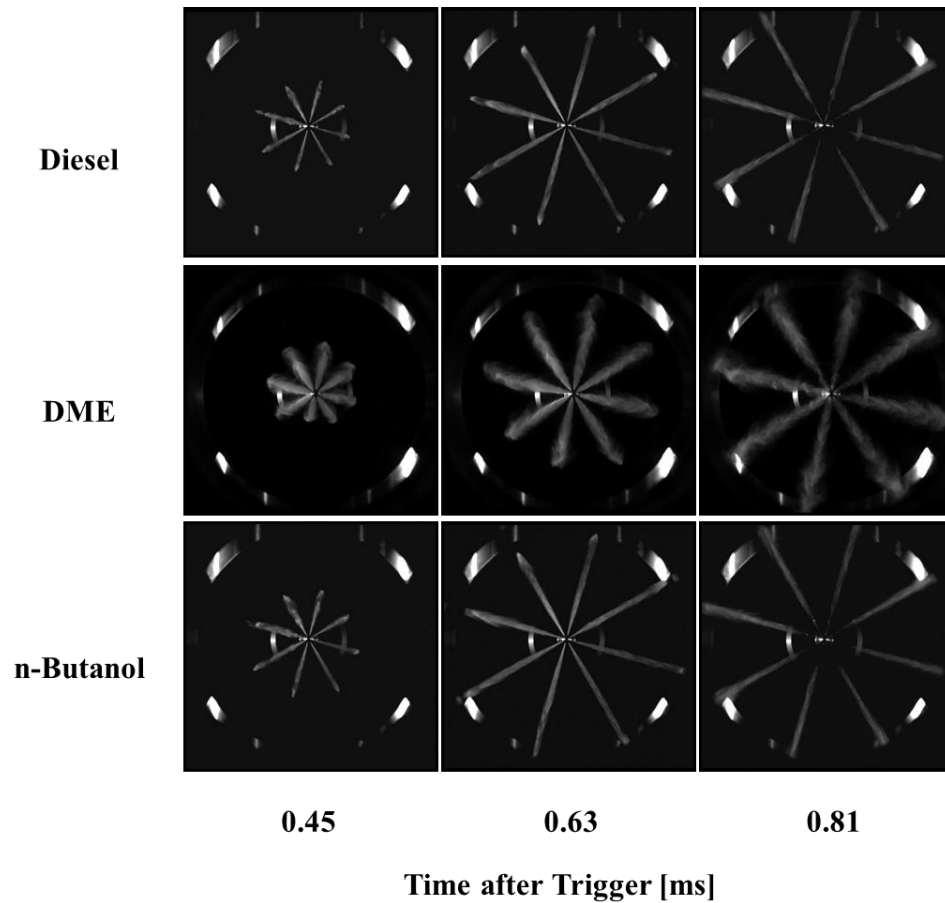
Figure 4.1 Direct fuel spray images of diesel, DME, and n-butanol at 450 bar injection pressure and 1 bar absolute background pressure

Further proven in correlation with Figure 4.2, DME presents spray characteristics unlike those of diesel and n-butanol fuel. At 450 bar injection pressure, the spray tip velocity of DME fuel is approximately 15-20% less than that of diesel fuel. Due to the low viscosity and surface tension of DME, a wider spray cone angle is observed in comparison with n-butanol and diesel. DME exhibits a spray cone angle around 2.5 times that of diesel spray.
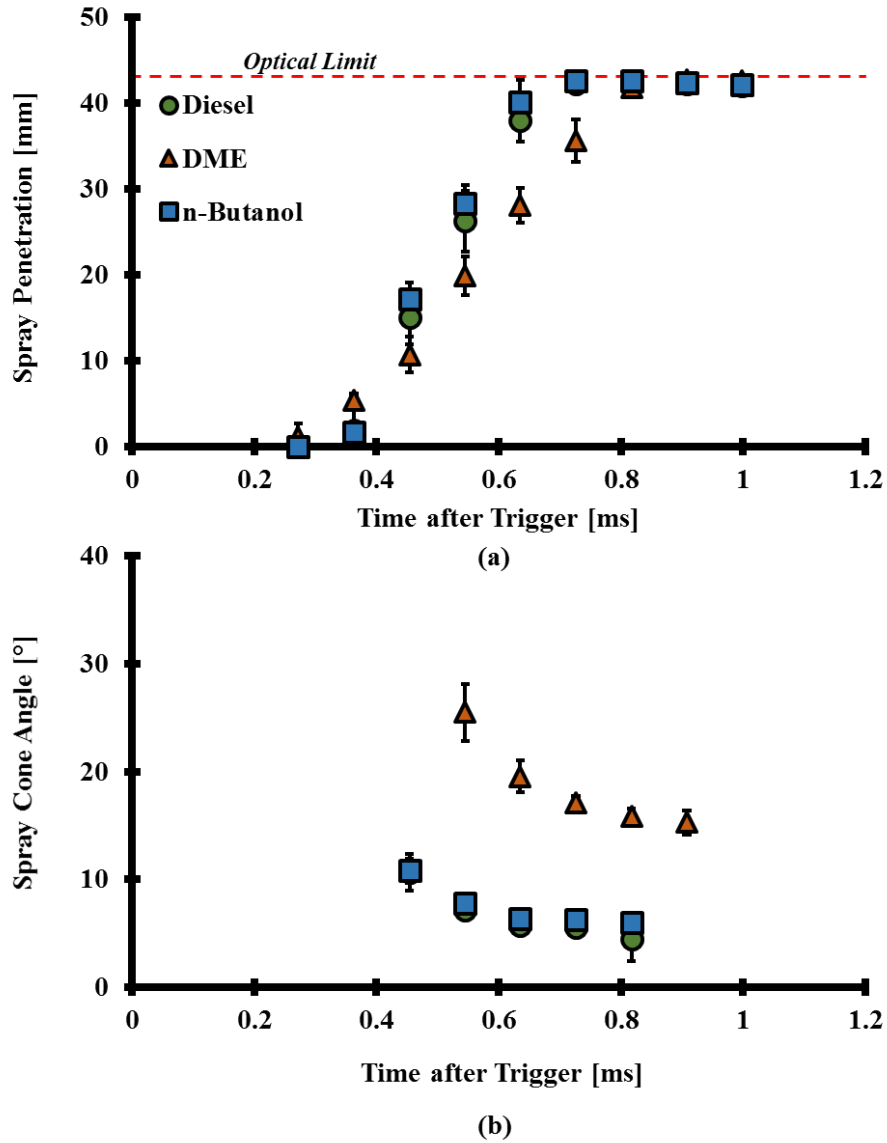
Figure 4.2 Spray characteristics of diesel, DME, and n-butanol fuel at 450 bar injection pressure and 1 bar absolute background pressure

Further investigations involve an injection of 900 bar. The fuel spray images and spray characteristics are shown in Figure 4.3 and Figure 4.4, respectively. In general, DME fuel exhibits the shortest spray penetration length and widest spray cone angle, which is consistent with prior conclusions. However, the differences among the three fuels converge

slightly when subjected to 900 bar injection pressure. The maximum deviation in spray

penetration length between DME and diesel lessens from ~10 mm to 3.2 mm.
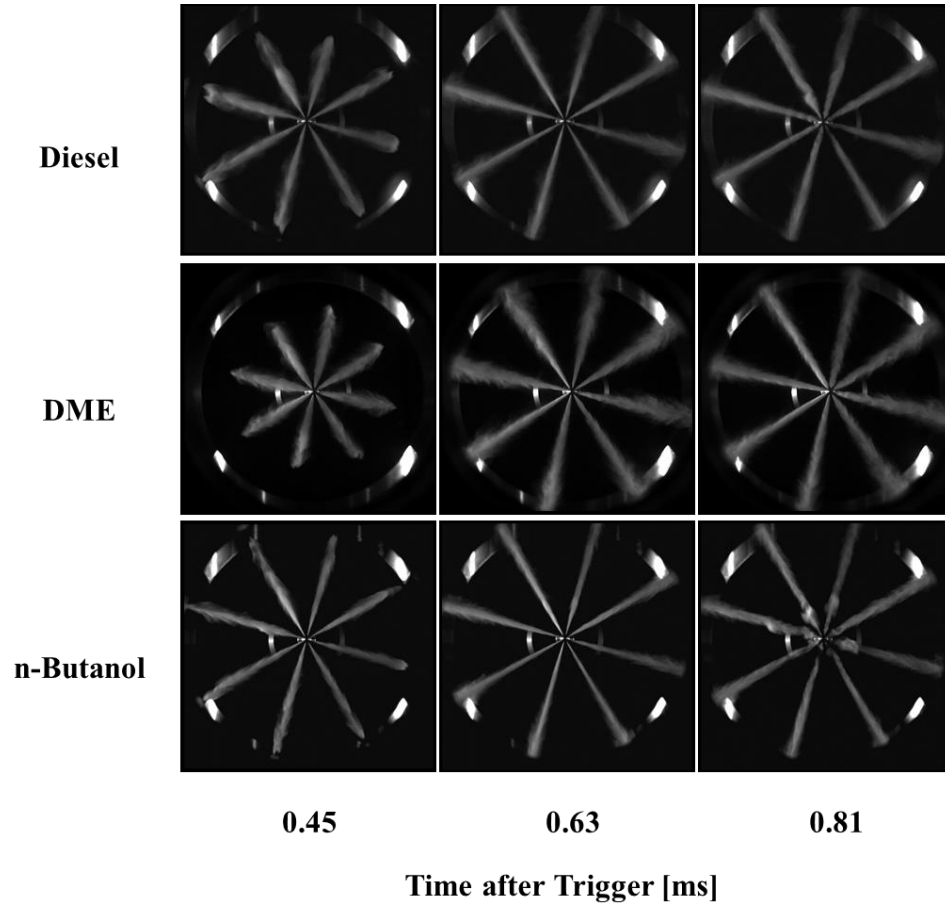
Figure 4.3 Direct fuel spray images of diesel, DME, and n-butanol at 900 bar injection
pressure and 1 bar absolute background pressure
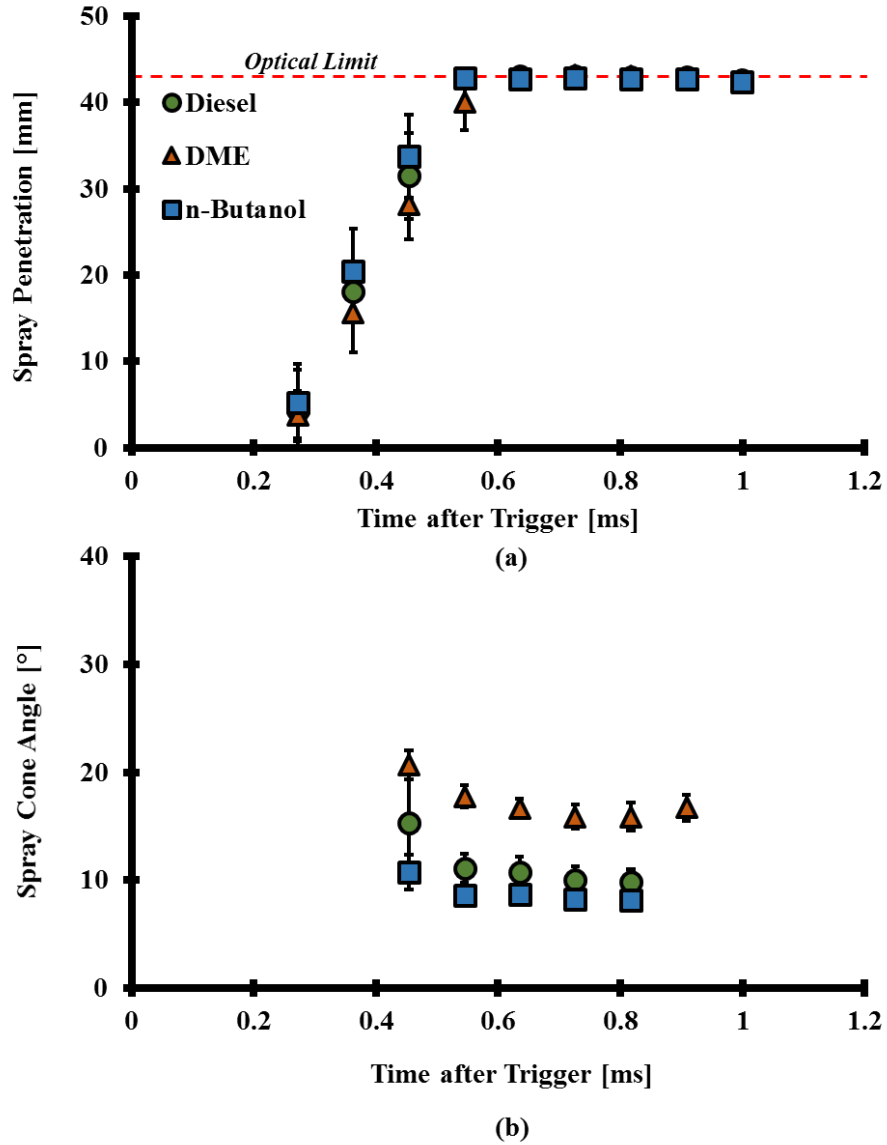
Figure 4.4 Spray characteristics of diesel, DME, and n-butanol fuel at 900 bar injection pressure and 1 bar absolute background pressure

4.1.2 Background Pressure

Efforts in this section are made to investigate the spray behaviour of DME, diesel, and n-butanol fuel injection at two injection pressures, 450 and 900 bar. The background pressure for which the fuel is injected into is controlled at 51 bar absolute. The images and spray characteristics are presented in Figure 4.5 and Figure 4.6, respectively. Contrary to the

significant differences in spray characteristics realized in Chapter 4.1.1 under 1 bar absolute background pressure, resemblances among the three fuels are prevalent when injected into a 51 bar absolute background pressure environment. The spray penetration lengths exhibit similar behaviour among the three fuels, while differences among the spray cone angles are more noticeable. The atomization behaviour of DME is faster than that of diesel and n-butanol. Because of this fast atomization characteristic, the standard deviation values for DME fuel spray cone angles are observed to increase beyond 1.27 ms after the trigger.
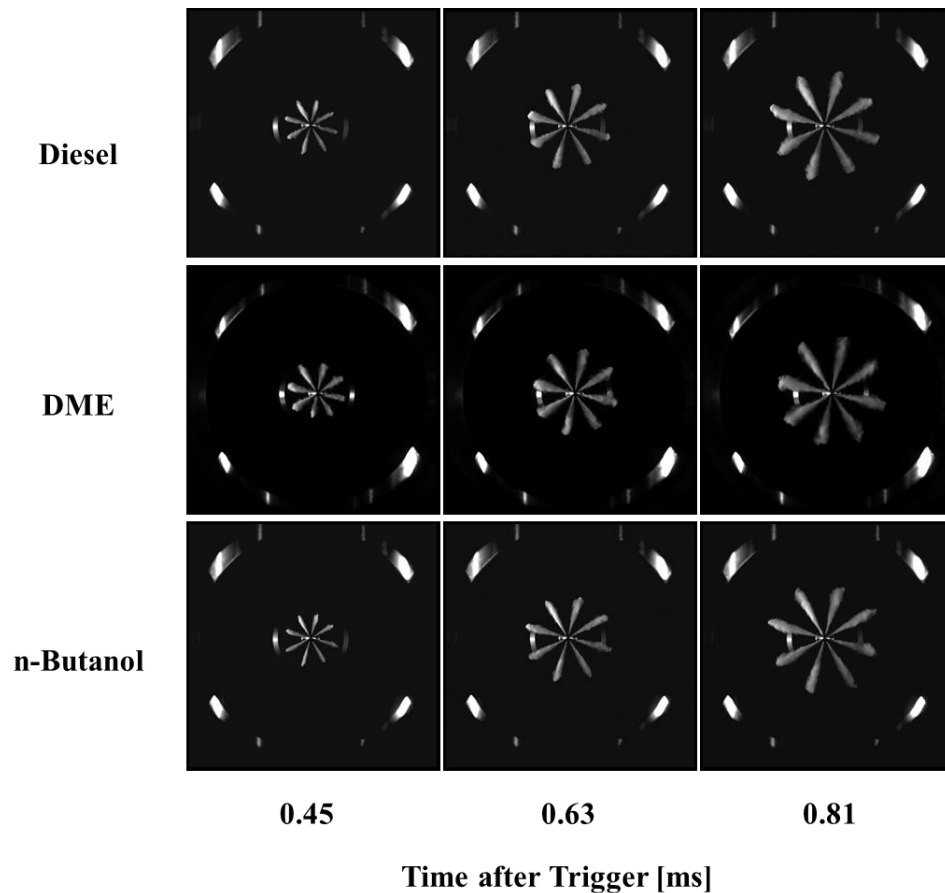
Figure 4.5 Direct fuel spray images of diesel, DME, and n-butanol at 450 bar injection pressure and 51 bar absolute background pressure
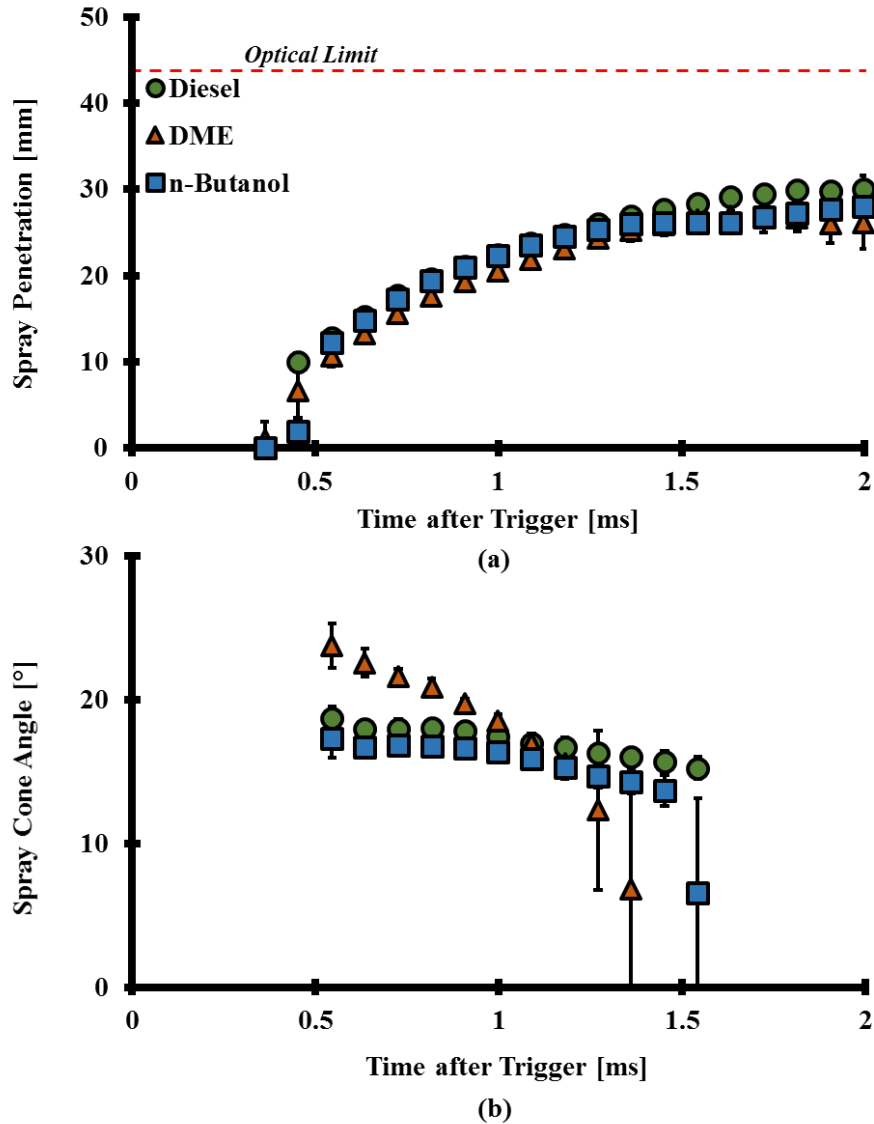
Figure 4.6 Spray characteristics of diesel, DME, and n-butanol fuel at 450 bar injection pressure and 51 bar absolute background pressure

To further assess the impact of background pressure on spray characteristics, the injection pressure is increased to 900 bar. The captured images and the derived spray characteristic values are shown in Figure 4.7 and Figure 4.8, respectively. The differences observed under 1 bar absolute background pressure in Chapter 4.1.1 are abridged when the background pressure is increased to 51 bar absolute. The maximum differences in the spray penetration

length among the three selected fuels has reduced from 5.5 mm to 3.6 mm. The maximum

differences in cone angle values among the three fuels have reduced from 10° to 2°.
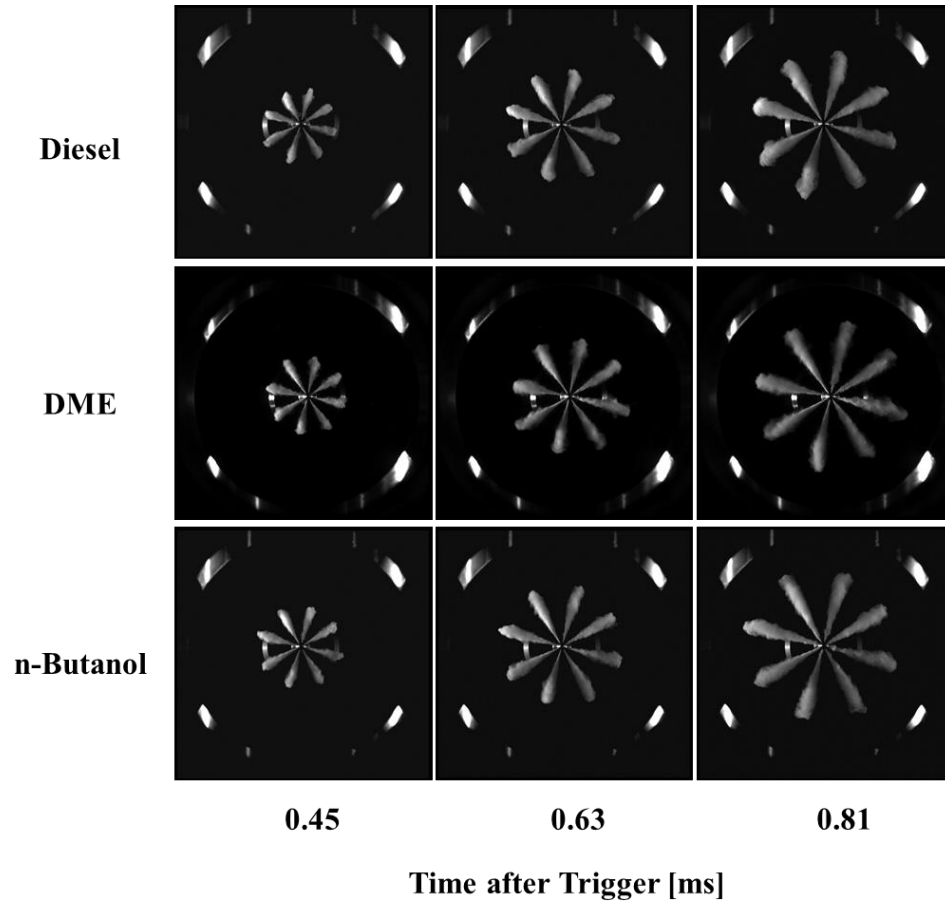
Figure 4.7 Direct fuel spray images of diesel, DME, and n-butanol at 900 bar injection
pressure and 51 bar absolute background pressure
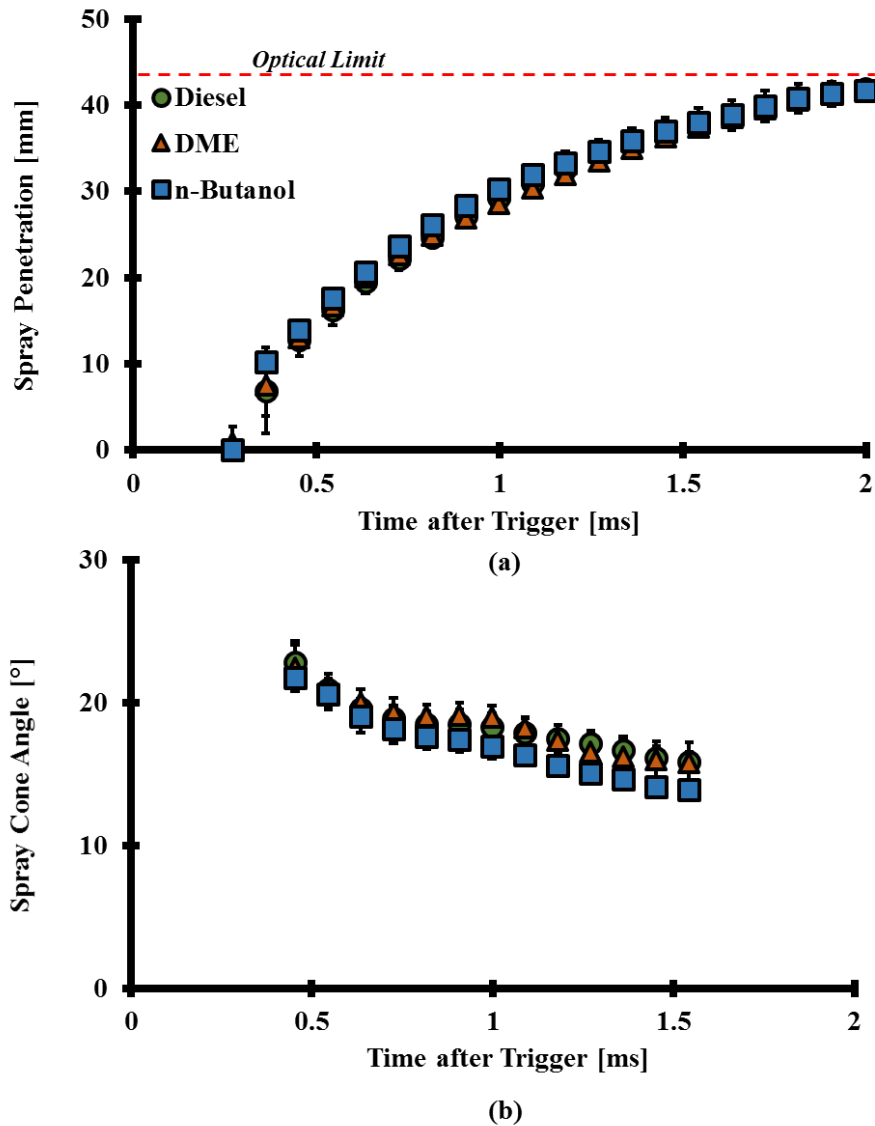
Figure 4.8 Spray characteristics of diesel, DME, and n-butanol fuel at 900 bar injection pressure and 51 bar absolute background pressure

4.2 Vaporization

The vaporization behaviours of diesel and DME fuel are analyzed in this section via a shadowgraph technique. The premise of this technique is detailed in Chapter 3.2. For this study, the injection pressure is maintained at 600 bar while background pressures of 1 and 31 bar absolute are employed. The ensuing diesel and DME fuel sprays under 1 bar absolute

background pressure are shown in Figure 4.9. It can be observed that more vaporization effects are observed with the DME fuel spray than that of diesel fuel.
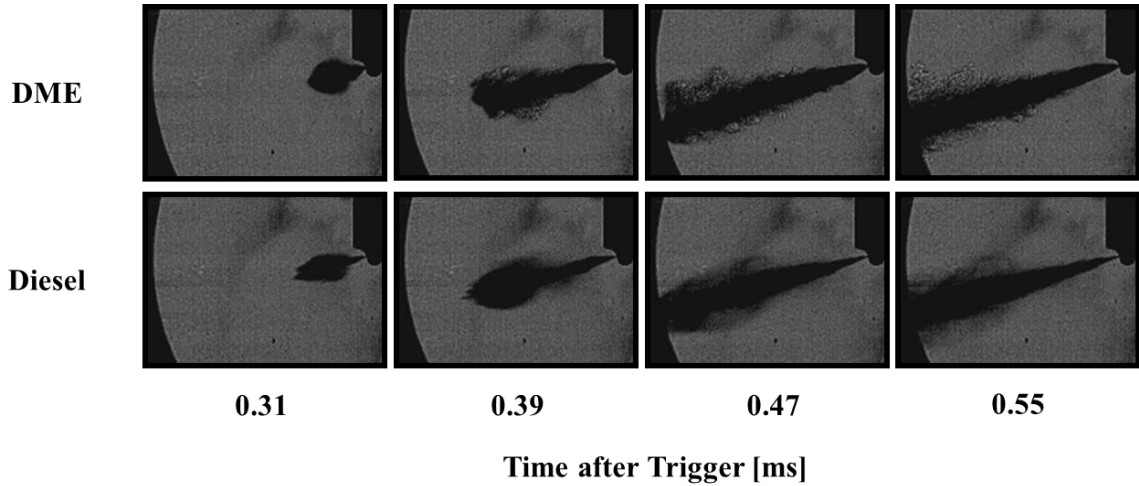
Figure 4.9 Shadowgraph fuel spray images of DME and diesel at 600 bar injection pressure and 1 bar absolute background pressure

The vaporization behaviour of the DME fuel spray is more prevalent under 31 bar absolute background pressure, as shown in Figure 4.10. Furthermore, the more vaporization is present around the DME fuel spray than that of the diesel fuel spray. The diesel injection exhibits a liquid-dominant injection, whereas the DME fuel exhibits vaporization around the contour of the spray. The vaporization is more perceptible as the spray penetrates. The increased vaporization in the DME fuel spray suggests that reaching a homogeneous fuel and air mixture will be relatively quicker than using diesel fuel.

DME

Diesel

| 0.31 | 0.50 | 0.69 | 0.88 |

Time after Trigger [ms]
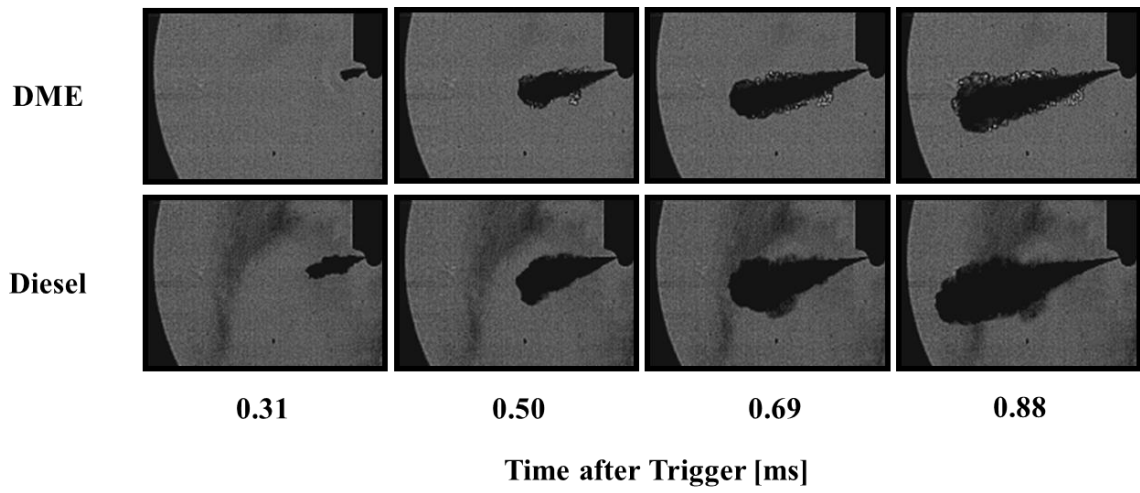
Figure 4.10 Shadowgraph fuel spray images of DME and diesel at 600 bar injection
pressure and 31 bar absolute background pressure

CHAPTER V

SUMMARY OF THESIS WORK

The objective of this work is to analyze the spray characteristics of dimethyl ether (DME) fuel injection at high-pressures. Moreover, the results are compared with other suitable fuels for direct injection (DI). A wide range of injection and background parameters were changed to allow for a thorough investigation of DME fuel spray. The experiments are conducted inside two different constant-volume chambers (CVC) to analyze the spray characteristics and the vaporization behaviour of fuel throughout the injection process.

5.1 Dimethyl Ether

Based on the results, the impacts of control parameters on the spray characteristics for DME fuel injection are as follows:

1. The spray penetration is largely dependent on the injection pressure and the background pressure conditions. The background gas density is increased with the background pressure, which, in turn, affects the spray penetration length. The spray penetration length increases with an increase in injection pressure or a decrease in background pressure.

2. The spray cone angle is not affected by the injection pressure. The cone angle is increased with an increase in background pressure.

3. Under 1 bar absolute background pressure, the fuel spray behaviour of DME is drastically changed under elevated background temperature conditions. DME injection under high background temperatures results in a wide cone angle, owing to the flash

boiling phenomenon. Under elevated background pressures, the flash boiling effects are mitigated as a result of the increase of the fuel boiling point (recall Equation 3.2).

4. The vaporization around the edges of the plumes can be observed with a shadowgraph imaging technique. It was observed that DME exhibits vaporization around the contours of the spray plume when subjected to 31 bar absolute background pressure. These findings are true for background pressures above 11 bar absolute.

5.2 Fuel Comparison

The feasibility of DME in a direct injection application can be linked to its similarities to popular fuels. The conclusions can be summarized as follows:

5. Under 1 bar absolute background pressure, DME spray exhibits a slower and wider spray than the fast, sharp, and narrow spray characteristics observed for diesel and n-butanol.

6. Under 51 bar absolute background pressure, the differences in spray penetration length and cone angle converge, resulting in similar spray characteristics.

5.3 Future Work

1. Conduct single-cylinder research engine (SCRE) experiments with direct injection DME. This will be used as baseline results, detailing a recommended injection timing, fuel quantity, output emissions, and resulting loads. The pressurized fuelling system must be a closed-loop and fabricated with DME-safe materials such as Teflon.

2. Expand on the range of tested parameters. A higher background temperature can be used to better represent the in-cylinder environment that can be expected during injector operation.

3. Detail the rate of injection (ROI) of DME. A Bosch long tube injection test bench should be used to perform the tests. It is important to quantify the injector delays (opening and closing delays and the fuel injection amount based on injection parameters.

REFERENCES

[1] R. Kumar, "Modeling, Control, and Implementation of Enhanced Premixed Combustion in Diesel Engines," University of Windsor.

[2] X. Han, M. Zheng, and J. Wang, "Fuel Suitability for Low Temperature Combustion in Compression Ignition Engines," *Fuel*, vol. 109, pp. 336–349, 2013.

[3] U. Asad and M. Zheng, "Efficiency & Stability Improvements of Diesel Low Temperature Combustion through Tightened Intake Oxygen Control," *SAE Int J Engines*, vol. 3, no. 1, pp. 788–800, 2010.

[4] J. B. Heywood, *Internal Combustion Engine Fundamentals*. New York, USA: McGraw-Hill, 1988.

[5] U. Asad, M. Zheng, X. Han, G. T. Reader, and M. Wang, "Fuel Injection Strategies to Improve Emissions and Efficiency of High Compression Ratio Diesel Engines," *SAE Int J Engines*, vol. 1, no. 1, pp. 1220–1233, 2008.

[6] S. Kook, C. Bae, P. C. Miles, D. Choi, and L. M. Pickett, "The Influence of Charge Dilution and Injection Timing on Low-Temperature Diesel Combustion and Emissions," *SAE Tech. Pap.*, 2005.

[7] M. Zheng, U. Asad, G. T. Reader, Y. Tan, and M. Wang, "Energy efficiency improvement strategies for a diesel engine in low-temperature combustion," *Int. J. Energy Res.*, vol. 33, no. 1, pp. 8–28, 2009.

[8] W. Chen, Z. Huang, and X. Lu, "A fundamental study on the control of the HCCI combustion and emissions by fuel design concept combined with controllable EGR . Part 2 . Effect of operating conditions and EGR on HCCI combustion," *Fuel*, vol. 84, pp. 1084–1092, 2005.

[9] U. Asad and M. Zheng, "Efficacy of EGR and Boost in Single-injection Enabled Low Temperature Combustion," *SAE Tech. Pap.*, 2009.

[10] S. Shafiee and E. Topal, "When will fossil fuel reserves be diminished?," *Energy Policy*, vol. 37, no. 1, pp. 181–189, Jan. 2009.

[11] X. Han, P. Divekar, G. Reader, M. Zheng, and J. Tjong, "Active Injection Control for Enabling Clean Combustion in Ethanol-Diesel Dual-Fuel Mode," *SAE Int. J. Engines*, vol. 8, no. 2, pp. 890–902, Apr. 2015.

[12] X. Han, "Study of fuels and fuelling strategies for enabling clean combustion in compression ignition engines," Electronic Theses and Dissertations, University of windsor, 2014.

[13] P. S. Divekar, "Clean Combustion Control in a Compression Ignition Engine," University of Windsor, 2016.

[14] J. Gieshoff, A. Schäfer-Sindlinger, P. C. Spurk, J. A. A. Van Den Tillaart, and G. Garr, "Improved SCR Systems for Heavy Duty Applications," *SAE Tech. Pap. Ser.*, 2000.

[15] G. R. Chandler *et al.*, "An Integrated SCR and Continuously Regenerating Trap System to Meet Future NOx and PM Legislation," *SAE Tech. Pap. Ser.*, 2000.

[16] M. Jeftić and M. Zheng, "Lean NOx trap supplemental energy savings with a long breathing strategy," *Proc. Inst. Mech. Eng.*, vol. 227, no. 3, 2012.

[17] A. Russell and W. S. Epling, "Diesel Oxidation Catalysts," *Catal. Rev.*, vol. 53, no. 4, pp. 337–423.

[18]   Z. Huang, X. Qiao, W. Zhang, J. Wu, and J. Zhang, "Dimethyl ether as alternative fuel for CI engine and vehicle," *Front. Energy Power Eng. China*, vol. 3, no. 1, pp. 99–108, 2009.

[19]   X. Han, T. Gao, U. Asad, K. Xie, and M. Zheng, "Empirical Study of Simultaneously Low NOx and Soot Combustion With Diesel and Ethanol Fuels in Diesel Engine," *J. Eng. Gas Turbines Power*, vol. 134, no. 11, 2012.

[20]   P. Divekar, Q. Tan, X. Chen, and M. Zheng, "Characterization of Exhaust Gas Recirculation for Diesel Low Temperature Combustion," *IFAC-Pap.*, vol. 48, no. 15, pp. 45–51, 2015.

[21]   A. Maiboom, X. Tauzia, and J.-F. Hétet, "Experimental Study of Various Effects of Exhaust Gas Recirculation (EGR) on Combustion and Emissions of an Automotive Direct Injection Diesel Engine," *Energy*, vol. 33, no. 1, pp. 22–34, 2008.

[22]   M. Zheng, X. Han, and G. T. Reader, "Empirical Studies of EGR Enabled Diesel Low Temperature Combustion," *J. Automot. Saf. Energy*, vol. 1(3), no. 3, pp. 219–228, 2010.

[23]   N. Ladommatos, S. Abdelhalim, and H. Zhao, "The Effects of Exhaust Gas Recirculation on Diesel Combustion and Emissions," *Int. J. Engine Res.*, vol. 1, no. 1, pp. 107–126, 2000.

[24]   "Alternative Fuels Data Center," *U.S. Department of Energy | Energy Efficiency & Renewable Energy*. [Online]. Available: https://afdc.energy.gov/fuels/properties.

[25]   T. Yanai, X. Han, M. Wang, G. T. Reader, M. Zheng, and J. Tjong, "Clean Combustion in a Diesel Engine Using Direct Injection of Neat n-Butanol," *SAE Tech. Pap.*, Apr. 2014.

[26]   T. A. Semelsberger, R. L. Borup, and H. L. Greene, "Dimethyl ether (DME) as an alternative fuel," *J. Power Sources*, vol. 156, no. 2, pp. 497–511, Jun. 2006.

[27]   C. Arcoumanis, C. Bae, R. Crookes, and E. Kinoshita, "The potential of di-methyl ether (DME) as an alternative fuel for compression-ignition engines: A review," *Fuel*, vol. 87, no. 7, pp. 1014–1030, 2008.

[28]   "Dimethyl Ether," *Gas Encyclopedia Air Liquide*. 2019.

[29]   J. Patten and T. McWha, "Dimethyl Ether Fuel Literature Review," National Research Council Canada. Automotive and Surface Transportation, ST-GV-TR-0032, Jun. 2015.

[30]   W. Ying and Z. Longbao, "Performance and Emissions of a Compression-Ignition Engine Fueled with Dimethyl Ether and Rapeseed Oil Blends," *Energy Fuels*, vol. 21, no. 3, pp. 1454–1458, 2007.

[31]   Z. Junjun, Q. Xinqi, W. Zhen, G. Bin, and H. Zhen, "Experimental Investigation of Low-Temperature Combustion (LTC) in an Engine Fueled with Dimethyl Ether (DME)," *Energy Fuels*, vol. 23, no. 1, pp. 170–174, 2009.

[32]   S. H. Park, H. J. Kim, and C. S. Lee, "Macroscopic spray characteristics and breakup performance of dimethyl ether (DME) fuel at high fuel temperatures and ambient conditions," *Fuel*, vol. 89, no. 10, pp. 3001–3011, 2010.

[33]   J. Yu, J. Lee, and C. Bae, "Dimethyl Ether (DME) Spray Characteristics Compared to Diesel in a Common-Rail Fuel Injection System," *SAE Tech. Pap. Ser.*, 2002.

[34]   C. K. Westbrook, W. J. Pitz, and H. J. Curran, "Chemical Kinetic Modeling Study of the Effects of Oxygenated Hydrocarbons on Soot Emissions from Diesel Engines," *J. Phys. Chem. A*, vol. 110, no. 21, pp. 6912–6922, 2006.

[35]   H. Ogawa, N. Miyamoto, and M. Yagi, "Chemical-Kinetic Analysis on PAH Formation Mechanisms of Oxygenated Fuels," *SAE Tech. Pap. Ser.*, p. 11, 2003.

[36]   S. H. Park and C. S. Lee, "Applicability of dimethyl ether (DME) in a compression ignition engine as an alternative fuel," *Energy Convers. Manag.*, vol. 86, pp. 848–863, Oct. 2014.

[37]   Y. Sato, S. Nozaki, and T. Noda, "The Performance of a Diesel Engine for Light Duty Truck Using a Jerk Type In-Line DME Injection System," *SAE Tech. Pap. Ser.*, Jun. 2004.

[38]   "California Dimethyl Ether Multimedia Evaluation - Tier 1," The University of California, 2015.

[39]   T. H. Fleisch, A. Basu, M. J. Gradassi, and J. G. Masin, "Dimethyl Ether: A fuel for the 21st Century," *Nat. Gas Convers. IV*, pp. 117–125, 1997.

[40]   A. J. Butler, "Propellants and refrigerants based on Trfluoro Propene 54," 3,884,828.

[41]   *DME Handbook Supplement*. Tokyo : Japan DME Forum, 2011.

[42]   X. Han, Z. Yang, M. Wang, J. Tjong, and M. Zheng, "Clean combustion of n-butanol as a next generation biofuel for diesel engines," *Appl. Energy*, vol. 198, pp. 347–359, 2017.

[43]   X. Han, M. Zheng, J. S. Tjong, and T. Li, "Suitability Study of n-Butanol for Enabling PCCI and HCCI and RCCI Combustion on a High Compression-ratio Diesel Engine," *SAE Tech. Pap.*, Sep. 2015.

[44]   S. S. Merola, C. Tornatore, S. E. Iannuzzi, L. Marchitto, and G. Valentino, "Combustion process investigation in a high speed diesel engine fuelled with n-butanol diesel blend by conventional methods and optical diagnostics," *Renew. Energy*, vol. 64, pp. 225–237, 2014.

[45]   G. Valentino, F. E. Corcione, S. E. Iannuzzi, and S. Serra, "Experimental study on performance and emissions of a high speed diesel engine fuelled with n-butanol diesel blends under premixed low temperature combustion," *Fuel*, vol. 92, no. 1, pp. 295–307, Feb. 2012.

[46]   Z.-H. Zhang and R. Balasubramanian, "Influence of butanol addition to diesel–biodiesel blend on engine performance and particulate emissions of a stationary diesel engine," *Appl. Energy*, vol. 119, pp. 530–536, Apr. 2014.

[47]   B. Choi *et al.*, "Effect of diesel fuel blend with n-butanol on the emission of a turbocharged common rail direct injection diesel engine," *Appl. Energy*, vol. 146, pp. 20–28, May 2015.

[48]   T. Yanai, G. Bryden, S. Dev, G. T. Reader, and M. Zheng, "Investigation of ignition characteristics and performance of a neat n-butanol direct injection compression ignition engine at low load," *Fuel*, vol. 208, pp. 137–148, Nov. 2017.

[49]   S. H. Park and C. S. Lee, "Combustion performance and emission reduction characteristics of automotive DME engine system," *Prog. Energy Combust. Sci.*, vol. 39, no. 1, pp. 147–168, 2013.

[50]   M. I. Khan, T. Yasmin, and A. Shakoor, "Technical overview of compressed natural gas (CNG) as a transportation fuel," *Renew. Sustain. Energy Rev.*, vol. 51, pp. 785–797, 2015.

[51]   J. Wu, Z. Liu, B. Wang, and J. Pan, "Measurement of the Critical Parameters and the Saturation Densities of Dimethyl Ether," p. 5.

[52]	M. Lapuerta, R. García-Contreras, J. Campos-Fernández, and M. P. Dorado, "Stability, Lubricity, Viscosity, and Cold-Flow Properties of Alcohol−Diesel Blends," *Energy Fuels*, vol. 24, no. 8, pp. 4497–4502, 2010.

[53]	E. Catizzone, G. Bonura, M. Migliori, F. Frusteri, and G. Giordano, "CO2 Recycling to Dimethyl Ether: State-of-the-Art and Perspectives," *Molecules*, vol. 23, no. 1, p. 31, Dec. 2017.

[54]	J. Yin, J. Wu, X. Meng, and I. Abdulagatov, "Compressed liquid density measurements of dimethyl ether with a vibrating tube densimeter," *J. Chem. Thermodyn.*, vol. 43, no. 9, pp. 1371–1374, Sep. 2011.

[55]	J. W. Hadley, G. C. Owen, and B. Mills, "Evaluation of a High Frequency Reciprocating Wear Test for Measuring Diesel Fuel Lubricity," *SAE Tech. Pap. Ser.*, 1993.

[56]	A. H. Lefebvre and V. G. McDonell, *Atomization and sprays*, Second edition. Boca Raton: CRC Press, 2017.

[57]	P. Werlberger and W. P. Cartellieri, "Fuel Injection and Combustion Phenomena in a High Speed DI Diesel Engine Observed by Means of Endoscopic High Speed Photography," *SAE Tech. Pap. Ser.*, p. 14, 1987.

[58]	J. Yu and C. Bae, "Dimethyl ether (DME) spray characteristics in a common-rail fuel injection system," *Proc. Inst. Mech. Eng. Part J. Automob. Eng.*, vol. 217, no. 12, pp. 1135–1144, 2003.

[59]	S. C. Sorenson, M. Glensvig, and D. L. Abata, "Dimethyl Ether in Diesel Fuel Injection Systems," *SAE Tech. Pap. Ser.*, 1998.

[60]	H. K. Suh and C. S. Lee, "Experimental and analytical study on the spray characteristics of dimethyl ether (DME) and diesel fuels within a common-rail injection system in a diesel engine," *Fuel*, vol. 87, no. 6, pp. 925–932, 2008.

[61]	J. C. Dent, "A Basis for the Comparison of Various Experimental Methods for Studying Spray Penetration," *SAE Tech. Pap. Ser.*, 1971.

[62]	H. Hiroyasu and M. Arai, "Structures of Fuel Sprays in Diesel Engines," *SAE Tech. Pap. Ser.*, 1990.

[63]	G. D'Errico, T. Lucchini, F. Contino, M. Jangi, and X.-S. Bai, "Comparison of well-mixed and multiple representative interactive flamelet approaches for diesel spray combustion modelling," *Combust. Theory Model.*, vol. 18, no. 1, pp. 65–88, Jan. 2014.

[64]	J. Naber and D. L. Siebers, "Effects of Gas Density and Vaporization on Penetration and Dispersion of Diesel Sprays," *SAE Tech. Pap. Ser.*, 1996.

[65]	G. S. Settles, *Schlieren and Shadowgraph Techniques: Visualizing Phenomena in Transparent Media*. Berlin Heidelberg: Springer, 2001.

[66]	Y. A. Çengel and M. A. Boles, *Thermodynamics: An Engineering Approach*, 8th Edition. New York: McGraw-Hill Education, 2015.

[67]	G. M. Faeth, L.-P. Hsiang, and P.-K. Wu, "Structure and breakup properties of sprays," *Int. J. Multiph. Flow*, vol. 21, pp. 99–127, Dec. 1995.

[68]	Y. Zeng and C.-F. F. Lee, "An Atomization Model for Flash Boiling Sprays," *Combust. Sci. Technol.*, vol. 169, no. 1, pp. 45–67, 2001.

[69]	T. L. Brown, *Chemistry: The Central Science*, 14th edition. New York: Pearson, 2018.

APPENDICES

APPENDIX A: Processing Code

```
% SIMON LEBLANC, UNIVERSITY OF WINDSOR,
% CLEAN COMBUSTION ENGINE LABORATORY
% MODIFIED: MARCH 2019
%
% THIS CODE IS MEANT TO IMPORT DIRECT SPRAY IMAGES AND OUTPUT RESULTING
% PENETRATION LENGTH AND CONE ANGLES


clear all
clc
threshold=5;
```

Code

```
next_dp=1;
dp_num=[1:5]; %Desired data points

for j=1:length(dp_num)
  if next_dp==1;
    dp_cur=dp_num(j);

    warning('off', 'Images:initSize:adjustingMag');
    %Input Variables
    workingDir = uigetdir;
    pictures = dir(fullfile(workingDir, '*.bmp'));
    pictureDIR = struct2cell(pictures);
    imageNames=pictureDIR(1,:);

    pic_bkgrnd=imread([workingDir,'\',imageNames{1}]);
    initial_found_count=0;
    initial_spray =[];
    retry_centre = {'N'};
    centre_x = 360;
    centre_y = 360;
    centre_found =0;
    reflection_answer =1;
    pic_num_refl = 1;
    fps = 11019;
    resolution = 0.17416444607; %nominal resolution mm/pix

    for i=2:length(imageNames)
      %Import Current Picture
      if i<10
```

```
    pic_num = (['00',num2str(i)]);
elseif i>=10 && i<100
    pic_num = (['0',num2str(i)]);
else
    pic_num = num2str(i);
end

pic_name = ([workingDir,'\',imageNames{i}]);
pic_curr=imread(pic_name);

%Turn picture to pixels with threshold barrier and substract background
pix_curr=pic_curr;
pix_threshold=pix_curr>10;
pix_threshold=bwareaopen(pix_threshold, 2);
pic_curr(pix_threshold==0)=0;
pic_nobkgrnd=pic_curr-pic_bkgrnd;

[r,c]=size(pix_curr);
Imax=max(max(pix_curr));
Boundary=fBoundary_test(pic_nobkgrnd, threshold);
pic_nobkgrnd(Boundary==1)=Imax;
pix_outline = pic_nobkgrnd-pic_curr;
[row,col]=find(pic_nobkgrnd==Imax);

%Rotate pixel outline
z=imrotate(pix_outline,60);

[rows, columns]=size(z);
%Convert to Binary Image
for bin_I_row=1:rows
    for bin_I_col=1:columns
        if z(bin_I_row,bin_I_col) >0
            pic_rot_pix(bin_I_row,bin_I_col)=1;
        else
            pic_rot_pix(bin_I_row,bin_I_col)=0;
        end
    end
end

num_pix = size(find(pic_rot_pix)==1);
pic_rot_pix_mod = pic_rot_pix;

%Locate the centre of the plume to isolate everything around it
if num_pix(1) > 10 && centre_found == 0
    [xi,yi] = getpts(imtool(z));
    centre_x = round(xi(end),0);
    centre_y = round(yi(end),0);
    pic_rot_pix_mod(:,1:centre_x)=0;
    initial_spray = min(find(pic_rot_pix_mod(centre_y,:)==1));
end

cur_initial_spray = min(find(pic_rot_pix_mod(centre_y,centre_x:columns)==1))+centre_x;

%If either these cannot find start of spray, assume plume is missing
```

```matlab
if isempty(initial_spray)==1 || isempty(cur_initial_spray)==1
    plume_length_mm = 0;
    initial_found_count = 0;
    data_calc(1:6) = [0];
else
    initial_found_count =1;
    pic_rot_pix_mod(:,1:cur_initial_spray-1)=0;
    up_limit_row_count = 1;
    bot_limit_row_count = 1;
    for mod_I_col=cur_initial_spray:columns

        white_dot_row = find(pic_rot_pix_mod(:,mod_I_col)==1);
        white_dot_from_centre = white_dot_row-centre_y;

        lower_pos_row = find(white_dot_from_centre>0);
        below_array_dots = sort(abs(white_dot_from_centre(lower_pos_row)),'ascend');
        below_array_full_dots = sort(abs(white_dot_row(lower_pos_row)),'ascend');

        upper_pos_row = find(white_dot_from_centre<0);
        above_array_dots = sort(abs(white_dot_from_centre(upper_pos_row)),'ascend');
        above_array_full_dots = sort(abs(white_dot_row(upper_pos_row)),'descend');

        %Upper Limit
        if length(above_array_dots) > 1
            for dots=1:length(above_array_dots)
                full_row_sel=above_array_full_dots(dots);
                if pic_rot_pix_mod(full_row_sel-1, mod_I_col)==0
                    upper_lim_perim = full_row_sel;
                    break
                end
            end
            Upper_limit_array(up_limit_row_count,:) = [mod_I_col,upper_lim_perim];
            up_limit_row_count = up_limit_row_count + 1;
        end

        %Lower Limit
        if length(below_array_dots) > 1
            for dots=1:length(below_array_dots)
                full_row_sel=below_array_full_dots(dots);
                if pic_rot_pix_mod(full_row_sel+1, mod_I_col)==0
                    below_lim_perim = full_row_sel;
                    break
                end
            end
            Lower_limit_array(bot_limit_row_count,:) = [mod_I_col,below_lim_perim];
            bot_limit_row_count = bot_limit_row_count + 1;
        end

        if mod_I_col <= cur_initial_spray + 40
            upper_peak = upper_lim_perim;
            lower_peak = below_lim_perim;
        end

        if mod_I_col > cur_initial_spray + 40
```

```matlab
            if upper_lim_perim < upper_peak
                upper_peak = upper_lim_perim;
            elseif below_lim_perim > lower_peak
                lower_peak = below_lim_perim;
            end
        end


    u_p(mod_I_col,1) = upper_peak;
    u_p(mod_I_col,2) = upper_lim_perim;
    l_p(mod_I_col,1) = lower_peak;
    l_p(mod_I_col,2) = below_lim_perim;



    %Eliminate the Exterior
    for mod_I_row=1:rows
        if mod_I_row < upper_peak-1
            pic_rot_pix_mod(mod_I_row,mod_I_col)=0;
        elseif mod_I_row > lower_peak+1
            pic_rot_pix_mod(mod_I_row,mod_I_col)=0;
        end
    end


    %Spray Pentration
    [row_perim, col_perim] = find(pic_rot_pix_mod==1);
    furthest_dot = max(col_perim);
    plume_length_pix = furthest_dot-initial_spray;


    %Cone Angle
    curr_lim = [centre_y, initial_spray, mod_I_col, upper_lim_perim, below_lim_perim];
    dist_pix_x = curr_lim(3) - curr_lim(2);


    dist_pix_up_y(mod_I_col) = curr_lim(1) - curr_lim(4);
    angle_pix_up_y = atand(dist_pix_up_y(mod_I_col)/dist_pix_x);


    dist_pix_down_y(mod_I_col) = curr_lim(5) - curr_lim(1);
    angle_pix_down_y = atand(dist_pix_down_y(mod_I_col)/dist_pix_x);


    cone_angle_indiv(mod_I_col) = angle_pix_up_y + angle_pix_down_y;


end
imshow(pic_rot_pix_mod)

%Total Elimination
for eli_I_row=1:rows
    for eli_I_col=1:columns
        if eli_I_row < upper_peak-1
            pic_rot_pix_mod(eli_I_row,eli_I_col)=0;
        elseif eli_I_row > lower_peak+1
            pic_rot_pix_mod(eli_I_row,eli_I_col)=0;
        end
    end
end
```

```matlab
imshow(pic_rot_pix_mod)
if reflection_answer < 5 || pic_num_refl == i
    choice = menu('Is there unwanted reflection?', 'Yes', 'No', 'Picture with Reflection', 'Never');
    if choice == 1
        reflection_answer = 1;
    elseif choice == 2
        reflection_answer = 0;
    elseif choice == 3
        reflection_answer = 5;
        pic_num_refl = str2num(cell2mat(inputdlg('Which picture will have reflection?')));
    else
        reflection_answer = 5;
    end
end

if reflection_answer ==1
    [xiii,yiii] = getpts(imtool(pic_rot_pix_mod));
    choice_col = round(xiii(end),0);
    pic_rot_pix_mod(:,choice_col:columns) = 0;
    [row_perim, col_perim] = find(pic_rot_pix_mod==1);
    furthest_dot = max(col_perim);
    plume_length_pix = furthest_dot-initial_spray;

elseif reflection_answer == 0
    plume_length_pix = plume_length_pix;
end

ini_search_thresh=round(initial_spray+(plume_length_pix*0.25),0);%Start at 25% of total plume length
fin_search_thresh=round(initial_spray+(plume_length_pix*0.75),0);%End at 75% of total plume length
plume_length_mm = plume_length_pix*resolution;


Upper_ini_row_thresh = find (Upper_limit_array == ini_search_thresh);
Upper_fin_row_thresh = find (Upper_limit_array == fin_search_thresh);
Lower_ini_row_thresh = find (Lower_limit_array == ini_search_thresh);
Lower_fin_row_thresh = find (Lower_limit_array == fin_search_thresh);

% Different methods of cone angle - PROOF OF THESE VALUES ARE IN
% /analyzing_lin_fit_spray.m
cone_angle_max_array = sort(cone_angle_indiv(ini_search_thresh:fin_search_thresh),'descend');
cone_angle_max = cone_angle_max_array(1);
cone_angle_min = cone_angle_max_array(end);
cone_angle_mean = mean(cone_angle_max_array);


%If either these cannot find start of spray, assume plume is missing

if isempty(Upper_ini_row_thresh)==1 || isempty(Upper_fin_row_thresh)==1 || isempty(Lower_ini_row_thresh)==1 ||
isempty(Lower_fin_row_thresh)==1
        cone_angle_regr=0;% or cone_angle_mean;
        cone_angle_loc=0;
        plot_q=0;
    else
        loc_for_angle = round(((plume_length_pix/2)+initial_spray),0);
```

```matlab
        cone_angle_loc = cone_angle_indiv(loc_for_angle);
        Up_thresh = [Upper_ini_row_thresh(1),Upper_fin_row_thresh(1)];
        Up_row_values = [Upper_limit_array(Up_thresh(1):Up_thresh(2),1)];
        Up_pixel_loc = [Upper_limit_array(Up_thresh(1):Up_thresh(2),2)];
        Up_row_values_full = [Upper_limit_array(:,1)];
        Up_pixel_loc_full = [Upper_limit_array(:,2)];


        Low_thresh = [Lower_ini_row_thresh(1),Lower_fin_row_thresh(1)];
        Low_row_values = [Lower_limit_array(Low_thresh(1):Low_thresh(2),1)];
        Low_pixel_loc = [Lower_limit_array(Low_thresh(1):Low_thresh(2),2)];

        % NORMALIZE TO ORIGIN OF INITIAL SPRAY POINT
        centre_spray_point = [initial_spray, centre_y];
        norm_up_pix = centre_spray_point(2)-Up_pixel_loc;
        norm_up_pix_full = centre_spray_point(2)-Up_pixel_loc_full;

        norm_low_pix = centre_spray_point(2)-Low_pixel_loc;
        norm_x_up = Up_row_values-centre_spray_point(1);
        norm_x_up_full = Up_row_values_full-centre_spray_point(1);
        norm_x_low = Low_row_values-centre_spray_point(1);
        if isempty(norm_x_low)==1 || isempty(norm_x_up)==1
            cone_angle_regr=0;% or cone_angle_mean;
            cone_angle_loc=0;
            plot_q=0;
        else

            % Regression Linear Fit with passing through injection point
            % (normalized to be at origin (0,0))
            norm_reg_up = norm_x_up\norm_up_pix;
            norm_fit_up = norm_reg_up*norm_x_up;
            full_dist_up = [1:max(norm_x_up)]';
            norm_fit_full_up = full_dist_up*norm_reg_up*-1;

            norm_reg_low = norm_x_low\norm_low_pix;
            norm_fit_low = norm_reg_low*norm_x_low;
            full_dist_low = [1:max(norm_x_low)]';
            norm_fit_full_low = full_dist_low*norm_reg_low*-1;


            % Cone Angle
            angle_up = -1*atand(norm_fit_full_up(end)/length(full_dist_up));
            angle_low = atand(norm_fit_full_low(end)/length(full_dist_low));
            cone_angle_regr = angle_up + angle_low;

            % Back to on plot linear fit
            Lin_fit_up_spray = norm_fit_full_up + centre_spray_point(2);
            Lin_fit_low_spray = norm_fit_full_low + centre_spray_point(2);
            plot_q=1;
        end
end

imshow(pic_rot_pix_mod)
title(['Frame: ', num2str(i-1), '| Penetration: ', num2str(plume_length_mm), '| Angle: ', num2str(cone_angle_regr)]);
```

67

```matlab
            %line([x1 x2], [y1 y2])
            if plot_q==1;
                hold on
                h_low = line([initial_spray initial_spray+length(full_dist_low)],[centre_y Lin_fit_low_spray(end)]);
                h1 = line([initial_spray initial_spray+length(full_dist_up)],[centre_y Lin_fit_low_spray(end)]);
                h_up = line([initial_spray initial_spray+length(full_dist_up)],[centre_y Lin_fit_up_spray(end)]);
                penetration = line([furthest_dot furthest_dot],[0 rows]);
                set(h_low(1),'linewidth',2);
                set(h_up(1),'linewidth',2);
                set(penetration(1),'linewidth',2);
            end


            if centre_found == 0
                centre_found_ans = questdlg('Do you want to change the centre for the shape of the plume?', 'Yes', 'No');
                switch centre_found_ans
                    case 'Yes'
                        centre_found = 0;
                    case 'No'
                        centre_found = 1;
                end
            end


            data_calc = [plume_length_mm, cone_angle_regr, cone_angle_max, cone_angle_mean, cone_angle_loc, cone_angle_min];
        end

        frame = i-1;
        frame_timeline_us = round((frame/fps)*1e6,0);
        frame_timeline_ms = round((frame/fps)*1e3,3);


        data_output(i-1,:) = [frame, frame_timeline_us, frame_timeline_ms, data_calc];


        pause(1)
        close all
        imtool close all

    end

    Headers = {'Frame', 'Time [us]', 'Time [ms]', 'Penetration Length', 'Regr_Cone Angle', 'Max_Cone Angle', 'Mean_Cone Angle', 'Loc_Cone Angle',
'Min_Cone Angle'};
    Plume_Data = [Headers; num2cell(data_output)];


    Spray_Data{dp_cur,1}=Plume_Data;

    if j < length(dp_num)
        next_dp_ans = questdlg(['Do you want to continue to the next dp, dp', num2str(dp_num(j+1)), '?'], 'Yes', 'No');
        switch next_dp_ans
            case 'Yes'
                next_dp = 1;
                disp(['Next DP, DP',num2str(dp_num(j)+1), ', it is.'])
            case 'No'
                next_dp = 0;
                disp('Session is over.')
        end
```

```
        end
      end
    end
```

VITA AUCTORIS

NAME:	Simon LeBlanc
PLACE OF BIRTH:	Windsor, Ontario, Canada
YEAR OF BIRTH:	1995
EDUCATION:	University of Windsor, B.A.Sc., Windsor, Ontario, Canada, 2017
	University of Windsor, M.A.Sc., Windsor, ON, Canada, 2019

List of Publications

Refereed Publications:

1. **S. LeBlanc**, P. Divekar, X. Han, J. Tjong, T. Li, and M. Zheng, "Preliminary Testing of n-Butanol HCCI on High Compression Ratio Diesel Engines," SAE Technical Paper Series, 2019.

2. S. Yu, D. Shouvik, Y. Zhenyi, **S. LeBlanc**, X. Yu, X. Han, T. Li, M. Zheng, "Early Pilot Injection Strategies for Reactivity Control in Diesel-ethanol Dual Fuel Combustion," SAE Technical Paper Series, 2018.

Other Publications:

3. X. Yu, **S. LeBlanc**, and M. Zheng, "Extending the Load Limits of DME in an HCCI/SACI Engine," presented at the Combustion Institute Canadian Section, Calgary, Canada, 2019.

4. **S. LeBlanc**, Z. Yang, X. Yu, C. Ye, S. Yu, and M. Zheng, "Effect of Lean and Diluted Conditions on the Combustion Process using Multiple Ignition Strategies," presented at the Combustion Institute Canadian Section, Toronto, Canada, 2018.

Conference Presentations:

5. WCX SAE World Congress Experience, 2019

6. Combustion Institute Canadian Section, Toronto, Canada, 2018